Chromium mobility in ultramafic areas affected by mining activities in Barro Alto massif, Brazil: An isotopic study

Viviana Bolaños-Benítez, Eric van Hullebusch, Jean-Louis Birck, Jérémie Garnier, Piet N.L. Lens, Mickaël Tharaud, Cécile Quantin, Yann Sivry

Chromium mobility in ultramafic areas affected by mining activities in Barro Alto massif, Brazil: An isotopic study

Viviana Bolaños-Benítez[1,2,3], Eric D. van Hullebusch[1], Jean-Louis Birck[1], Jérémie Garnier[4], Piet N.L. Lens[3], Mickaël Tharaud[1], Cécile Quantin[5] and Yann Sivry[1*]

[1] *Université de Paris, Institut de physique du globe de Paris, CNRS, F-75005 Paris, France*
[2] *Université Paris-Est, Laboratoire Géomatériaux et Environnement (LGE), EA 4508, UPEM, 77454 Marne-la-Vallée, France*
[3] *Department of Environmental Engineering and Water Technology, IHE Delft Institute for Water Education, PO 3015, 2601 DA Delft, The Netherlands*
[4] *Universidade de Brasilia, IG/GMP-ICC Centro, 70919-970, Brasilia-DF, Brazil*
[5] *UMR 8148 GEOPS, Université Paris Saclay - CNRS, 91405 Orsay Cedex, France*

* Corresponding author: sivry@ipgp.fr

Abstract

This work studies the potential release of Cr from solids to surface water and groundwater, and the related isotopic compositions, in a nickel laterite ore deposit from Barro Alto in Brazil (in the State of Goiás). This ultramafic system is characterized by elevated concentrations of chromium (Cr). Even largely immobile Cr may be naturally leached from weathering profiles such as laterite to the surface and groundwater. This system is exploited for metal production, and both mining and metallurgical activities result in a significant increase in the trivalent (Cr(III)) and hexavalent chromium (Cr(VI)) concentrations released into the environment via runoff. Among all the samples collected, ores contained higher amounts of chemically and isotopically exchangeable Cr(VI) ($E_{Cr(VI)}$) with values as high as 104 (± 8) mg kg^{-1}. $\delta^{53}Cr$ increased from -0.28 (± 0.01)‰ to -0.05 (± 0.01)‰ and the $E_{Cr(VI)}$ value was up to 30 times higher in deep soils than at the surface (up to 7 (± 1) mg kg^{-1}). Chemically extracted Cr(VI) ($E_{Cr(VI)}$-KH_2PO_4) displayed positive $\delta^{53}Cr$ value (1.69 (±0.03) ‰) with a similar Cr isotopic composition as the ones measured in freshwater sampled in and around the mine area. It appears that Cr is primarily released as Cr(VI), i.e. the toxic species, and becomes increasingly more available as it moves from the soil profile to the ores and mining residues. Based on the differences in the Cr isotopic composition, this study proves that $\delta^{53}Cr$ can be used in environmental studies to trace Cr leaching.

Keywords: Chromium mobility, ultramafic area, isotopic fractionation, mining

1. Introduction

Redox reactions control changes in Cr speciation, and these reactions subsequently affect Cr isotopic ($\delta^{53}Cr$) variations in natural environments (Ellis et al., 2002; Schauble et al., 2004; Qin and Wang, 2017; Rivera et al., 2018). Chromium has two oxidation states, Cr(III) and Cr(VI), and four stable isotopes: ^{50}Cr (abundance 4.31%), ^{52}Cr (83.76%), ^{53}Cr (9.55%) and ^{54}Cr (2.38%). Organic material, sulfides, and ferrous species control the reduction of Cr(VI) to Cr(III) (Fendorf, 1995). During this reduction, the reaction rates of the light ^{52}Cr are faster and thereby the remaining Cr(VI) is isotopically enriched in ^{53}Cr (Schauble et al., 2004; Qin and Wang, 2017). Hydrolyzed Cr(III), can be slowly oxidized to the toxic and mobile Cr(VI), by reducing Mn oxides that are easily reducible (Leita et al., 2009; Vithanage et al., 2019). Cr isotopic fractionation is also caused by this process, and results in a residual Cr(III) that is depleted in ^{53}Cr and a mobile Cr(VI) enriched in heavy isotopes.

The weathering of ultramafic rocks, containing high amounts of Cr, releases Cr(VI) that is usually enriched in heavy Cr isotopes, with values reported up to $\delta^{53}Cr(VI)_{aq}$ = +3.9‰ (Farkaš et al., 2013). This Cr(VI) is then retained on positively charged minerals (Crowe et al., 2013) or leached towards the surface and groundwater (Izbicki et al., 2008; Trebien et al., 2011; Novak et al., 2014). Based on studies carried out in ultramafic areas in Brazil (Garnier et al., 2009b, 2008, 2006) and New Caledonia (Becquer et al., 2010, 2006, 2003), it is known that a fraction of Cr is exchangeable under the highly toxic anionic form Cr(VI). However, human activities (e.g. electroplating processes, and the tanning and chemical industry) can also release Cr, and these activities produce significantly higher Cr isotopic fractionation (5.8‰) when compared with Cr released from natural sources (Novak et al., 2017b, 2017a). Raous et al. (2013) found that ores and spoils from nickel mines (Barro Alto, Brazil) have a high concentration of exchangeable Cr(VI) (2% of the total Cr) and that these contents are highly affected by the hydrological conditions (Raous et al., 2010).

Studies of anthropogenic Cr sources usually focus on the release of Cr(VI) (Novak et al., 2017b, 2017a). However, not much is known about Cr(III) release due to human activities such as mining, where the access to the ore deposit implies soil cover removal and transport of large quantities of soil (Losfeld et al., 2014; Vithanage et al., 2019). Furthermore, nothing is known about the environmental relevance of isotopic fractionation, the processes causing it, or the isotopic composition of the materials found in ultramafic mining environments.

The present study was carried out to assess the impact of mining activities on the Cr isotopic composition of the material extracted in the mine, and its effect on Cr mobility in ultramafic areas. The studied site is a Ni-rich laterite deposit (Barro Alto, Goiás state, Brazil). Samples collected from a weathering cover were used to ascertain the degree of natural and human-induced weathering and its correlation with the Cr mobility and isotopic composition. This work also assesses the isotopic signature of Cr found in the material extracted from the mine, to determine whether Cr isotopes can be used as tracers of mining activities.

2. Field settings and sampling

2.1. Study site

The Barro Alto, Niquelândia and Caña Brava ultramafic complexes belong to a 350 km long belt found in the northern part of the State of Goiás (Brazil). Metamorphic volcanic-sedimentary sequences delimit the boundaries of the Barro Alto complex (Ferreira Filho et al., 1992). This complex is a large mafic-ultramafic layered intrusion that underwent granulite facies metamorphism. Researchers have shown that lateritic ores and limonite, in the Niquelândia and Barro Alto complexes, have high Cr contents with up to 6030 mg kg^{-1} (Ratié et al., 2015) and 46800 mg kg^{-1} (Raous et al., 2013), respectively. In ultramafic systems, Cr-rich magnetite ($Fe^{2+}(Fe^{3+}, Cr)_2O_4$), chromite ($FeCr_2O_4$), talc ($Mg_3Si_4O_{10}(OH)_2$), secondary Fe-oxyhydroxides and chlorite ($(Mg, Fe)_5$ $Al[(OH)_8$ $AlSi_3O_{10}]$) are all mineral phases that contain Cr (Fandeur et al., 2009; Garnier et al., 2009a; Oze et al., 2004). Although these materials are not rich enough in Cr to be extracted, they can potentially be harmful to the environment.

The Barro Alto mine (Figure 1) is located in the Barro Alto complex and occurs as an arc that spreads for 35 km in a southwest to northeast direction. The main mineral resource is saprolite that is overlain by laterites and which contains sequences of serpentinized dunites and pyroxenes that are surrounded by gabbros. The Barro Alto mine consists of an open-pit mine exploited since 2011 and a ferronickel plant operated by Anglo American (Raous et al., 2010; Ratié et al., 2016). The laterite and saprolite ore can be accessed without blasting and is loaded using excavators and mixed. Trucks are used to transport the ore to the plant's preparation yard where it is stored until a beneficiation process which includes crushing, calcination, smelting and refining (Moore, 2012).

105 *2.2. Sampling and conditioning of samples*

106 In June 2015, nine water samples were collected from streams, ponds and groundwater in and
107 around the Barro Alto mine (Goiás State, Brazil). Stream 1, used as a reference, is found outside
108 the mine in the ultramafic area, whereas mining activities had a direct impact on stream 2. Three
109 sediment ponds are used within the mine to store runoff water and to discourage the leaching of
110 particles. Four piezometers were used to collect groundwater both upstream and downstream
111 the mine (Piezo 1 and 2, respectively) and upstream and downstream the smelter area (Piezo 3
112 and 4, respectively, Figure 1). There was no rain right before the samples were taken. Each
113 sample collected contained roughly one liter of water, stored in acid-cleaned polyethylene
114 bottles. On-site *in situ* measurements were taken using a WTW 3410 Set 2 multi-parameter
115 probe, including temperature, pH and electrical conductivity. Some part of the bulk samples were
116 filtered through a pre-cleaned 0.7 µm Whatman™ grade GF/F glass microfiber filter and the
117 suspended particulate matter was retained for analysis. The filtrate was split into two parts:
118 H_3PO_4 was added to the first part, which was stored in amber glass bottles, to lower the pH for
119 the dissolved organic carbon (DOC) analysis. The second part was directly stored for the anion
120 analysis. The remaining bulk samples were filtered using a PES (Polyethersulfone) syringe filter
121 with a 0.22 µm pore size. Ultrapure concentrated HNO_3 was added to acidify the samples for the
122 total major and trace element analyses. All of the samples, i.e. filtered acidified and non-
123 acidified, were stored at 4°C.
124
125 Ores, sediments and bedrocks samples and two soil profiles were also collected in June 2015.
126 Soil profile 1 (S1) consists of three layers (0-10 cm, 10-40 cm and 80-100 cm) and soil profile 2
127 (S2) consists of two layers (0-15 cm and 15-40 cm). The samples taken in the mine exploitation
128 area include eight lateritic (OL1 – OL8) and three saprolitic (OS1 – OS3) ores. The bottom
129 sediment samples were collected in stream 2 (Se1), pond 1 (Se2) and pond 2 (Se3) (Figure 1).
130 The three bedrock samples (B1, B2 and B3) respectively correspond to a serpentinite collected
131 in the area (B1) and to two samples taken at the base of two separate cores at respective
132 depths of 27 m and 28 m (B2 and B3). The mining company Anglo American had previously
133 drilled through the cores to the lateritic regolith. The two latter samples are the same as those
134 studied by Ratié et al. (2018): samples R C26-27 and R C27-28. The solid samples were first
135 dried at atmospheric temperature, sieved with a 2 mm sieve (except for the rocks) and stored in
136 polypropylene plastic bags. A marble mortar was used to crush soils, ores and sediments as well
137 as to homogenize the resulting powder. The rocks were crushed in a ceramic jaw crusher and
138 an agate mill was used to reduce them to powder.

2.3. Samples digestion

Approximately 0.05 g of powdered soils, ores, sediments and rocks were dissolved in a solution combining 2 mL concentrated ultrapure distilled HNO_3 and 1 mL HF. This mixture was heated on a hotplate for 48 hours at 100°C. The samples were then dried and, to dissolve the fluorides, they were flushed with aqua regia (3:1 HCl:HNO_3). Next, the samples were dried and then dissolved in 1 mL of 6N HCl. If black residues could still be observed (common in samples that contain certain minerals such as chromite), the dissolved fraction was extracted, thereby leaving the black residue and to which a volume of 100 µL of $HClO_4$ was added. This solution was placed on a hot plate at 120°C for 24 h, and once dissolved, the $HClO_4$ was evaporated in an evapoclean (Analab) closed low temperature evaporation system. The residue itself was dissolved in 6N HCl and mixed with the original dissolved fraction to perform the trace elements and isotope analysis. Samples taken from the river, ponds and groundwater were evaporated and the residue subsequently dissolved in 1 mL 6N HCl. The SPM that had been collected on the filters was removed and dissolved using the same procedure described above for the solid samples.

3. Methods

3.1. Chemical analyses

A Panalytical MiniPal 4 energy-dispersive X-Ray fluorescence (EDXRF) benchtop spectrometer (Rh X-Ray tube-30kV-9W) was used to analyze the total metal content in the solid samples at a resolution of 150 eV (Mn Kα). Measurements were taken as per the thin-layer hypothesis. The bauxite standard BX-N was used to determine the quality of the analysis. A PANalytical grazing incidence X-ray diffraction (GIXRD) diffractometer was used to determine the mineralogical composition using Cu Kα radiation (at 45kV – 40 mA) in the 5°-70° 2θ range with a scan step of 0.013°.

The anion (F^-, Cl^-, NO_3^-, SO_4^{2-}) concentrations in the water samples were measured using ion chromatography (ICS 1100, Thermo Fisher) equipped with a Thermo Scientific IonPac AS14 analytical column and a Thermo Scientific IonPac AG14 pre-column. A flow rate of 1.2 mL min^{-1} was used to inject 20 µL of the mobile phase (a mixture of Na_2CO_3 and $NaHCO_3$). Shimadzu's total organic carbon TOC-V_{CSH} analyzer was used to analyze the dissolved organic carbon (DOC) concentrations. The major element concentrations (Fe, Mn, Al, Cr, Ni, Na, K, Mg, Ca, Si) were measured in all the samples after a first dilution in 2% ultrapure HNO_3 using ICP-AES

(ICAP 6200, Thermo Fisher). High-Resolution ICP-MS (Element II, Thermo Scientific) with multi-element standard solutions were used to measure concentrations below 10 µg L^{-1}. The ICP-AES generally has detection limits that range from 10 to 200 µg L^{-1}. The detection limits for the ICP-MS are typically between 0.006 and 0.074 µg L^{-1}. The measurements had standard deviations (1σ) lowers than 5%.

3.2. Isotopic analyses

Aliquots of acid digested samples were used to purify the Cr purification as per the measured concentrations and the cation exchange resin method (Birck and Allegre, 1988; Trinquier et al., 2008). A Biorad AG 50WX8 cation exchanger was used to run two successive elutions which involved first dissolving the samples in 0.1N HCl and then passing them through the resin. The Cr was immediately collected right after loading. Then, any Cr still presents in the sample was completely eluted by adding 5 mL 1N HCl. The next step was to add 2 mL of 6N HCl to the resin. The resulting fraction was collected, evaporated and once again dissolved in 0.1N HCl. This fraction was then passed again through the resin, as described above. Then, to dissolve the residue, 60 µL of 16 N HNO_3 was added to the mixed and evaporated Cr fractions from the two elutions. Next, 2 mL of Milli-Q water was added and the mixture was heated to 100°C for a period of 24 hours. When the sample was completely cool, it was passed through a column of the same size as above. This load was discarded. The residual Ti, Na and Al were eliminated by adding 5 mL of 0.5N HF and 22 mL of 1N HCl. Lastly, 10 mL of 2N HCl was added to elute the Cr. Between each elution, 15 mL of 6N HCl was used to wash the columns. Ninety-five percent (± 5%) of the elution was recovered (i.e. representing the yield). To eliminate the HCl, the samples were evaporated until dry and once again dissolved in 0.6% HNO_3.

A Multicollector ICP-MS (Neptune, Thermo Scientific), located at the Institut de Physique du Globe de Paris (IPGP), was used to measure the chromium isotopic compositions. The purified Cr samples were dissolved in 0.5% HNO_3 with Cr concentrations of 100 ppb and 50 ppb for the solid and water samples, respectively. A PFA µFlow nebulizer (at a flow rate of 100 µL/min) coupled with an Elemental Scientific's desolvating nebulization system (APEX-IR), without additional gas or membrane desolvation, was used to introduce the diluted samples into the plasma. Under high-resolution mode, a sensitivity of 2.8-4.9 V on ^{52}Cr was obtained per 100 ppb Cr with the use of jet sample and H skimmer cones. Faraday cup detectors connected to amplifiers with 10^{11} Ω feedback resistors were implemented to measure all of the ion beams. The possible isobaric interferences of ^{50}Ti, ^{50}V and ^{54}Fe were corrected by measuring and

monitoring the ^{49}Ti, ^{51}V and ^{56}Fe isotopes. To monitor the potential drift, the unprocessed NIST SRM 979 standard was analyzed after running each set of three samples. These results show that there was minimal drift within each analytical session (< 0.1%). The on-peak blanks were measured before and after every sample/standard for correction purposes. The assessment of the analytical accuracy and precision involved the repeated processing and measurement of the USGS reference material BHVO-2 standards (-0.11 ± 0.02‰, 2SD, n = 3).

In line with previous studies on Cr isotopes, the δ notation (see equation (1) was used to express the $^{53}Cr/^{52}Cr$ ratio. This notation is a per mil deviation from NIST SRM 979 (the standard reference material):

$$\delta^{53}Cr(‰) = \left[\left(\frac{^{53}Cr/^{52}Cr_{sample}}{^{53}Cr/^{52}Cr_{SRM\ 979}}\right) - 1\right] * 1000 \quad \textbf{(1)}$$

3.3. Chromium mobility

3.3.1. Isotopic exchange

The isotopically exchangeable pool of Cr(VI), $E_{Cr(VI)}$-Spike, was determined by using a $^{50}Cr(VI)$ spike purchased in its oxide form from ISOFLEZ USA and certified with a 96.5% abundance in $^{50}Cr(VI)$ when the natural ^{50}Cr abundance is 4.345%. The chromium oxide was first dissolved in 6N HCl and evaporated before adding the $HClO_4$. The solution was heated at a temperature of 190°C over a period of two days. The spike solution was evaporated in the evapoclean and then dissolved once again in 16N HNO_3 before dilution with Milli-Q water. At the end of this procedure, a stock solution of 100 mg L^{-1} of $^{50}Cr(VI)$ was obtained.

The soil suspensions contained 1 g of the sample (< 2 mm) mixed with 10 mL of Milli-Q water and 10 µL of 24.8 mg L^{-1} NaN_3 used as a biocide. This mixture was placed in an end-over-end shaker for 48 h. The second step involved adding 10 µL of the spike solution to the suspensions and then shaking the samples for one more day, before filtration using a 0.22 µm PES (Polyethersulfone) filter. Given that the spike solution has a low pH, a maximum of 10 µL of the spike was added to each sample to not change the chemical equilibrium. The filtrate was diluted with 2% HNO_3.

In natural systems, no significant isotope exchange between Cr species occurs over a period from several days to several weeks (Zink et al., 2010; Wang et al., 2015), whereas isotopes are exchanged between Cr(VI) species within 24 hours (Garnier et al., 2009b). Therefore, one can

assume that the isotopic equilibrium results from the exchange between the added ^{50}Cr(VI) and the labile natural Cr(VI) species and that the measurement of the isotopic signature in the filtrate provides direct information about the (isotopically) exchangeable pool of Cr(VI).

High-Resolution ICP-MS (Element II, ThermoScientific) was used to determine the isotopic ^{50}Cr, ^{52}Cr, ^{53}Cr and ^{54}Cr abundances in the filtrates, spike solution and unspiked sample. Analyses run on other isotopes, e.g. ^{47}Ti, ^{51}V and ^{57}Fe were used to correct the isobaric interferences for ^{50}Cr and ^{54}Cr. The isotopic ratio was calculated based on the average of 20 runs for which the analytical reproducibility is higher than 1% (2SD, n = 520). To verify and correct, if necessary, the drifts in signal and intensity, the samples were divided into blocks bracketed with unspiked solutions and standard Cr solutions.

The ratio between ^{50}Cr and ^{52}Cr, i.e. the two most abundant isotopes in the suspension, was used to determine the pool of isotopically exchangeable Cr ($E_{Cr(VI)\text{-}spike}$). Equation (2) (Zelano et al., 2016) was used to calculate the $E_{Cr(VI)}$ – spike (mg kg^{-1}) value:

$$E_{Cr(VI)-spike} = Q * \frac{M_{STD}}{M_S} * \frac{A_S}{A_{STD}} * \left[\frac{(I.R.)_{Spike} - (I.R.)_{Sample}}{(I.R.)_{Sample} - (I.R.)_{UN}}\right] \quad \textbf{(2)}$$

where Q is the volume of spike added (µg of spike per kg of the sample), M_{STD} and M_S are the atomic masses of Cr (g mol^{-1}) in the standard and spike solutions, respectively, and A_{STD} and A_S are the percentage of ^{52}Cr abundances in the standard and spike solutions, respectively. Both the un-spiked solutions ($(I.R.)_{UN}$) and the sample ($(I.R.)_{Sample}$) were analyzed to determine their respective isotopic abundances. In the sequence of analysis, triplicate samples were bracketed with their correspondent unspiked solution and the spikes and blanks were analyzed to monitor the signal, isotopic abundances and possible cross-contaminations.

3.3.2. Chemical extraction

The chemically exchangeable Cr(VI) and Cr(III) pools, called $E_{Cr(VI)}$-KH_2PO_4 and $E_{Cr(III)}$-KCl, were assessed using 0.1 M KH_2PO_4 and 1 M KCl, respectively. A solution containing 1 g of soil and 25 mL of the reactant was shaken for 1 h (Garnier et al., 2006). The supernatant was placed in a centrifuge for 15 min at 2500 rpm and then filtered through a 0.22 µm PES membrane to separate the supernatant. Concentrations of Cr in the latter were determined by ICP-AES and High-Resolution ICP-MS.

4. Results

4.1. Characterization of soils, ores, sediments and rocks

Table 1 provides the chemical and mineralogical characteristics of the bedrocks, ores, soils and sediments studied in the present work. The mineralogy of bedrock B1 is dominated by serpentine with trace amounts of chromite, while B2 and B3 are also comprised of chlorite and olivine. Si and Mg occur in the highest amounts in B1, B2 and B2. Their respective contents varied between 188 and 194 g kg^{-1}, and between 183 and 156 g kg^{-1}. In bedrocks B2 and B3, Al, Cr and Mn had an average content of 1.2, 1.3 and 1.0 g kg^{-1}, respectively.

Although lateritic ores display high content of Fe, ranging from 85 to 536 g kg^{-1}, saprolitic ores contain more Si than Fe, with values reaching 167 g kg^{-1}. The third most abundant element found in lateritic ores is aluminum with contents between 14 and 70 g kg^{-1}. Contents in the saprolitic ores were found to be 18 g kg^{-1} for OS1, 16 g kg^{-1} for OS2 and 14 g kg^{-1} for OS3, indicating that this element is more variable in lateritic ores. Lateritic (OL1-OL8) and saprolitic (OS1-OS3) ores are characterized by iron mineral phases that contain both hematite and goethite. The saprolitic ores also contain Mg, which could be related to the occurrence of serpentine. Saprolites contain quite high contents of Ni (between 22 g kg^{-1} and 32 g kg^{-1}). Lower nickel contents are found in laterite, except for ores OL2 (22 g kg^{-1}), OL4 (22 g kg^{-1}) and OL6 (21 g kg^{-1}). Lateritic ores contain higher Cr contents (10-19 g kg^{-1}) compared to saprolitic ores (ores OL3, OL2 and OL1 have respective values of 3, 4 and 4 g kg^{-1}).

The soil1 (S1) and soil2 (S2) profiles show Fe contents between 250 and 281 g kg^{-1} and between 272 and 330 g kg^{-1}, respectively. The Cr content for S1 ranges from 10 to 12 g kg^{-1} and 16 to 12 g kg^{-1} in S2. Both Fe and Cr occur in higher contents in the first layer (0-15 cm) of both soil profiles. The other mineral phases present, if the Fe(III) oxides and Fe(III) (oxy)hydroxides (i.e. hematite) are not considered, are chlorite and quartz. Soil profile S2 also contains chromite and magnetite. Further down in the S1 soil (at a depth of 80-100 cm), contents of Al are higher (79 g kg^{-1}) compared to the superficial soils (74 g kg^{-1}), while in soil profile S2 Al contents are higher at the surface (77 g kg^{-1}). The reverse trend is found for Fe and Cr. The S1 soil profile shows that the contents of both Ni (with an average content of 6 g kg^{-1}) and Mn (4 g kg^{-1} on average) remain stable along the soil profile. Compared to S1, the contents of Ni (9 g kg^{-1}) and Mn (11 g kg^{-1}) are higher in the surface soil of S2. The contents of the elements found in the sediment ponds, in decreasing order, are as follows: Fe (202-332 g kg^{-1}), followed by Mg (66-86 g kg^{-1}), Al (11-44 g kg^{-1}), Ni (9-17 g kg^{-1}), Cr (3-9 g kg^{-1}) and Mn (3-4 g kg^{-1}). The dominant

minerals in the sediments are iron oxides (goethite and hematite), serpentine, clinochlore and quartz, which correspond to the mineralogy found in the ore and overburden (soil) deposits from the Barro Alto mine.

4.2. Exchangeable chromium pool

Higher amounts of the chemically extracted Cr(VI) ($E_{Cr(VI)}$-KH_2PO_4) are found in ores, sediments and soils, compared with chemically extracted Cr(III) ($E_{Cr(III)}$-KCl) (Table 2). In the ore samples, the $E_{Cr(VI)}$-KH_2PO_4 pool ranges from 1 to 104 mg kg^{-1} (Figure 2), whereas $E_{Cr(III)}$-KCl varies between 0.2 and 10 mg kg^{-1}. Ponds 1 and 2 sediments (Se2 and Se3) have $E_{Cr(VI)}$-KH_2PO_4 values of 10 and 2.4 mg kg^{-1}, which are higher than the value of 1.2 mg kg^{-1} obtained for stream 2 sediments (Se1). For the soil profiles, the $E_{Cr(VI)}$-KH_2PO_4 values are close to 30 times lower for samples taken at depths within the first 10 cm compared to up to 100 cm (0.7 mg kg^{-1} versus 21 mg kg^{-1}). The same pattern is observed for $E_{Cr(III)}$-KCl, with values starting at 0.39 mg kg^{-1} in the shallower soil layer (10-40 cm) and increasing to 3.7 mg kg^{-1} in the 80-100 cm layer (i.e. the deepest one).

Figure 2 compares the chemically ($E_{Cr(VI)}$-KH_2PO_4) and the isotopically exchangeable pool of Cr ($E_{Cr(VI)\text{-}spike}$). In the ores, sediments and soils, there is a positive correlation between $E_{Cr(VI)}$-KH_2PO_4 and $E_{Cr(VI)\text{-}spike}$ (R^2 = 0.9). It has been shown that the reactive metal content in soils can be accurately measured, in a reproducible manner, by diluting the stable isotope (Marzouk et al. 2013). This measurement provides more information than a single extraction procedure. Based on this statement, $E_{Cr(VI)}$-KH_2PO_4 sampled at depths ranging between 10 and 40 cm is under-estimated in saprolitic ores and soil 1 (S1). However, for the saprolite ores, the presence of sub-micrometer colloidal particles (SCPs) may explain the difference between the $E_{Cr(VI)}$-KH_2PO_4 pool compared to the one-one line (Bolaños-Benítez et al., 2018; Lombi et al., 2003; Marzouk et al., 2013), as these particles are comprised of non-isotopically exchangeable metals and may result in over-estimated $E_{Cr(VI)\text{-}spike}$. The total Cr content can be broken down into a non-mobile reservoir of Cr(III), making up 99% of this total content, and an exchangeable pool of Cr(VI) comprising the remaining 1%. Cr(III) could be oxidized and mobilized in freshwater systems.

4.3. Water chemistry

The physicochemical characterization of the samples collected is presented in Table 3. The highest electrical conductivity values, 167 µS cm^{-1} and 292 µS cm^{-1} respectively, are found in samples of groundwater collected from the piezometers located upstream of the mine (Piezo 1) and the smelter (Piezo 3). These values respectively decrease to 155 µS cm^{-1} and 48 µS cm^{-1} in

339 the piezometers located downstream from the mine (Piezo 2) and the smelter (Piezo 4). There is
340 a simultaneous decrease in the concentrations of calcium and magnesium by 90% along with
341 decreases in the alkalinity (from 79 to 11 mg L^{-1}) and decreased pH neutralization capacity (from
342 6.6 to 5.7) throughout the smelter area. The groundwater samples taken from the piezometers
343 located at the smelter indicate that the concentrations of other elements, such as K and Na, also
344 decreased (by 62 and 63%, respectively).
345
346 In stream 1, the dissolved major elements are hereafter listed by their concentrations in
347 decreasing order: Mg^{2+} (12 mg L^{-1}), Ca^{2+} (3 mg L^{-1}) and Na^{+} (0.5 mg L^{-1}). In pond 2, the Mg^{2+} and
348 Ca^{2+} concentration is 13 mg L^{-1} and 5 mg L^{-1}, respectively. The present work shows that the
349 concentrations of the major elements generally decrease in the order $Mg^{2+} > Ca^{2+} > Na^{+} > K^{+}$ and
350 the anion concentrations decrease in the order NO_3^- or $SO_4^{2-} > Cl^- > F^-$. The highest SPM
351 concentrations (166 to 317 mg L^{-1}) were found in the ponds. These concentrations are up to 30
352 times higher than those determined in fresh and groundwater (Table 3). Ponds 1, 2 and 3 exhibit
353 dissolved Cr concentrations of 757, 58 and 89 µg L^{-1}, respectively. Due to the release of Cr from
354 waste materials coming from the mine, the concentration of Cr is 130 times higher in stream 2
355 than in stream 1 (13 µg L^{-1} versus 0.1). The Cr concentration in the groundwater is higher
356 upstream the mine (2.4 µg L^{-1}) and the smelter (1.1 µg L^{-1}) than downstream (0.2 µg L^{-1}).
357
358 The groundwater of the mining area had slightly higher DOC concentrations that observed in the
359 other areas with concentrations of 3.74 mg L^{-1} for piezometer 1 and 4.65 mg L^{-1} for piezometer
360 2. Table 3 shows that higher particulate carbon concentrations are found in groundwater
361 sampled before and after the smelter area (6.51% and 9.63%, respectively) compared to
362 groundwater in the mine (5.84% on average). The particulate organic carbon content determined
363 in the freshwater varied between 0.64 and 3.65wt% (Table 3).
364
365 *4.4. Cr isotopic composition*
366 Solid and liquid samples collected in the ultramafic area, both inside and outside the mining
367 area, were analyzed to determine the $\delta^{53}Cr$ values as these values help to identify the natural
368 and human-derived processes controlling Cr fate. The measured $\delta^{53}Cr$ values for all the samples
369 collected are given in Table 1 for solids and in Table 3 for liquids, and displayed in Figure 3.
370 Negative $\delta^{53}Cr$ values, related to a depletion of light Cr isotopes (Frei and Polat, 2013; Berger
371 and Frei, 2014; Qin and Wang, 2017), were found for certain solid samples such as lateritic ores
372 (-0.76 ± 0.07‰ to -0.24 (± 0.02)‰), soils (-0.28 (± 0.06)‰ to -0.10 (± 0.04)‰), sediments (-

373 0.77 (± 0.05)‰ to -0.22 (± 0.04)‰) and part of the SPM (-0.89 (± 0.01)‰ to -0.18 (± 0.07)‰). A
374 negative $\delta^{53}Cr$ value (-0.17 ± 0.01)‰ was found in bedrock B1, whereas this value is positive for
375 B2 and B3 (+0.18 (± 0.08)‰ and +0.10 (± 0.04)‰, respectively). The $\delta^{53}Cr$ values in the
376 saprolitic ores are positive and range from +0.93 (± 0.05)‰ to +1.05 (± 0.12)‰. Stream 2
377 (+0.94 (± 0.09) ‰) and the two piezometers located before (Piezo 1) (+0.65 (± 0.09) ‰) and
378 after (Piezo 2) (+0.93 (± 0.08) ‰) the mine record the highest $\delta^{53}Cr$ values for the SPM.
379
380 High $\delta^{53}Cr$ values, from +2.10 (± 0.13)‰ to +3.66 (± 0.04)‰, were found in the water samples.
381 The variation of these values is within the same range as that for the isotopic signatures
382 determined in Cr(VI) extracted with KH_2PO_4 from the ores OL1, OL3, OL5 and OL8 as well as
383 sediment samples Se1 and Se2, with values of $\delta^{53}Cr$ ranging from +1.34 (± 0.07)‰ to
384 +4.37 (± 0.06)‰ (Figure 3).
385
386 *5. Discussion*
387 *5.1. Weathering in tropical ultramafic environments*
388 Assuming that the mining activity in Barro Alto has had a significant effect on the natural
389 stratigraphic column, all the surface samples collected in this study may have originally held a
390 different position in that column. Based on the assumption that this position has a direct
391 relationship with the extent of alteration, the calculation of an index of alteration for bedrocks,
392 ores, soils and sediments can be used to reconstruct a theoretical stratigraphic column.
393 Babechuk et al. (2014) followed by Aiglsperger et al. (2016) have proposed to develop an
394 ultramafic index of alteration (UMIA). The UMIA accounts for the following: magnesia (MgO) and
395 silica (SiO_2) are dominant in ultramafic rocks whereas CaO, Na_2O, K_2O occur in very small
396 amounts. MgO and SiO_2 are depleted near the surface in the majority of Ni laterites while iron
397 and alumina oxides (Fe_2O_3 and Al_2O_3, respectively) are simultaneously enriched (Aiglsperger et
398 al., 2016). The following equation is used to calculate the UMIA:
399

$$UMIA = \frac{Al_2O_3 + Fe_2O_3}{Al_2O_3 + Fe_2O_3 + MgO + SiO_2} * 100 \quad \textbf{(3)}$$

400
401 The UMIA produces values between 0 and 100 and is used to identify incipient (UMIA < 20),
402 intermediate (UMIA= 20-60) or intense to extreme (UMIA > 60) mineralogical transformations.
403 Table 1 shows that, except for OL2, the lateritic ores have UMIA values higher than 60 (82-98),
404 indicating that an intense mineralogical transformation occurred and that the mobile elements
405 were leached. Accordingly, it is associated with Cr enrichment mainly as Cr(III). Our results are

similar to those found by Raous et al. (2013), who reported an enriched lateritic horizon in goethite, hematite and chromiferous spinel. Conversely, the UMIA values for saprolite ores and bedrock, ranging from 8 to 13, indicate an incipient degree of alteration (Table 1). Similar results were obtained by Rivera et al. (2018) who found UMIA values between 4 and 47 in the saprolitic and limonitic horizons. The less weathered saprolite sample resembles the bedrock content with a small degree of weathering, and the highest values were reached out in the limonitic horizons.

The saprolitic and lateritic ores in the soils have UMIA values between 47 and 62. Even though lateritic ores and soils have similar chemical compositions, soils have different mineralogy that includes hematite, chlorite and quartz. It is not surprising to find hematite, goethite, maghemite, and amorphous Fe (oxy)hydroxides in soils given that they are part of the soil-forming phases in serpentine soils (Coleman and Jove, 1993). However, it is possible to find quartz as a secondary mineral in lateritic regoliths found in soils covering ultramafic rocks (Vojcu and Bardoux, 1997). It seems likely that this quartz may come from eolian sources in the surrounding sites that are not ultramafic. Lastly, the UMIA values of the sediments indicated an intermediate mineralogical alteration. This result most likely has to do with the fact that sediments contain particles from various sources. This implies that these UMIA values represent the averages found in soils and ores.

The UMIA value interpretation was combined with an Al-Fe-Si-Mg molar ternary plot that illustrates the trend for mafic and ultramafic minerals (primarily serpentine) with regards to weathering. There is a clear weathering trend, as shown in Figure 4, from the less weathered to more weathered samples, i.e. from the bedrock to the lateritic ores. Compared to the bedrock, lateritic ores (OL1-OL8) are highly-enriched in Fe and Al. This is due to i) the strong leaching of alkali and Si during hydrolysis, and ii) the precipitation of secondary minerals such as Fe oxides, e.g. goethite and, to a lesser degree, hematite. Saprolitic ores (OS1, OS2 and OS3) contain small amounts of Al and Fe and are enriched in Mg, with serpentine and smectite as the main mineral phases (Table 1). The presence of Mg-bearing alteration minerals such as serpentine and talc, which can be formed in ultramafic rocks, may explain these Mg enrichments regardless of fact that chlorite is the main Mg-mineral phase in saprolite (Vojcu and Bardoux, 1997).

Table 1 shows that there is a low degree of alteration in the bedrocks (B1, B2 and B3). Samples of this type typically display high Mg contents and extremely low Al, Cr, Mn and Ni contents given that incipient weathering has occurred and therefore certain soluble elements, e.g. Mg, are

still present. The mineralogy assemblage contains serpentine and chlorite with trace amounts of chromite, amphibole and olivine. The content of the elements in these soils decreases in the order Fe > Al > Mg, indicating that these soils are found close to the lateritic ores. Conversely, for the sediments, the Mg content was higher than the Al content and Fe remained the dominant element (Table 1).

5.2. Chromium behavior during weathering

Figure 5(a) depicts a graph plotting the total Cr content in the samples against the ultramafic index of alteration (UMIA). The samples containing the lowest Cr contents (0.3-1.3 g kg^{-1}) and least-altered materials are the bedrock samples. This parent material undergoes weathering leading to the formation of lateritic and saprolitic ores and soils. The Cr content found in this type of weathering product depends on the degree of alteration as Cr is not very soluble, particularly when included in chromite. Lateritic ores, which have some of the highest Cr contents (from 10 to 19 g kg^{-1}), are among the most altered materials. The low solubility of Cr, compared with the highly leachable element from the bedrock such as Si and Mg, result in higher Cr contents in altered materials. Soils are also characterized by high levels of Cr (10-15 g kg^{-1}), whereas the average Cr content in saprolite is only 4 g kg^{-1}. Finally, sediments contain a mixture of both soils and ores (with a Cr content ranging from 3 to 9 g kg^{-1}) and are possibly the material that has been altered to a higher degree. As displayed in Figure 1, the sediments from pond 1, which collects the runoff from the ore extraction area, have a high Cr content (9 g kg^{-1}). Our results are very comparable with those of Paulukat et al. (2015) who published data on the total Cr content found in a weathering profile in an Odisha Mining Corporation-chromite mine (Sukinda Valley, India). These authors report a total Cr content ranging from 24 to 60 g kg^{-1} in the laterite, 33 g kg^{-1} in the saprolite and with significantly lower average contents of 7 g kg^{-1} in the bedrock.

The exchangeable pool of Cr(VI) is plotted against the UMIA in Figure 5(b) and shows that the highest content of exchangeable Cr(VI) is found in the most weathered material. This result is consistent with the oxidative weathering of rocks, during which Cr(III) is oxidized to Cr(VI). This oxidation is more likely to occur if compounds with high redox activities, such as elemental oxygen and manganese oxides and hydroxides, are present (Trebien et al., 2011). It is expected that the metals present in Mn oxides will be subjected to co-precipitation and substitution, particularly when alternating wetting and drying cycles occur in the soil (Essington, 2005 in Trebien et al., 2011). This is an essential step for laterite to form. Our results show that, except for soil 2 (S2) which is the only sample containing magnetite and chromite, there is a significant

positive correlation between Mn and Cr contents ($R^2 = 0.9$), and Mn content and UMIA ($R^2 = 0.8$). An identical correlation can be seen between the extracted Cr(VI) and the total Mn content, indicating that Mn is involved in the oxidation of Cr(III) and the subsequent production of the toxic Cr(VI) (Fendorf and Zasoski, 1992; Garnier et al., 2013; Rai et al., 1989). However, it should be noted that the amount of easily reducible Mn oxides present, and not only the total content of Mn, determines the extent of Cr(III) oxidation (Trebien et al., 2011).

Cr(VI) adsorption may occur through outer-sphere complexes (Fendorf, 1995) onto iron oxides which have a high point of zero net charge (PZNC), and they can effectively adsorb oxyanions such as Cr(VI) when the pH values fall between 2 and 7 (Zachara et al., 1989). Positive correlations are found for Fe and Cr in bedrock, saprolitic ores, lateritic ores, soils and sediments ($R^2 = 0.8$). As seen in Table 2, the highest contents of exchangeable Cr(VI) in the lateritic ore samples (12-104 mg kg^{-1}) are found in OL1, OL3, OL5, OL7 and OL8, which primarily contain Fe oxides. The remaining samples display a smaller $E_{Cr(VI)}$ range of variation concerning the previously described ores (0.7-21 mg kg^{-1}).

Tau (T) factors (Equation 4) are used to calculate mass balances, useful to quantify the mass gains and losses of individual chemical elements with regards to the bedrock (Rivera et al., 2018):

$$\tau_{Ti,Cr} = \frac{Cr_{sample}/Ti_{sample}}{Cr_{Bedrock}/Ti_{bedrock}} - 1 \qquad [4]$$

where Cr_{Sample} and $Cr_{Bedrocks}$ represent the total Cr content (in g kg^{-1}) present in both the samples and bedrock, respectively. Titanium, in the sample (Ti_{sample}) and bedrock ($Ti_{bedrock}$), was used as the immobile element to normalize the Cr content (Table 1). The samples have a higher Cr content compared to the bedrock, except the sediment samples from stream 2 (Se1) and pond 2 (Se3). In this latter, the negative tau values suggest that Cr is gradually lost. It has been demonstrated previously that isotopic fractionation may occur as a result of Cr enrichment or loss due to redox processes (Crowe et al., 2013; Frei and Polat, 2013; Wang et al., 2015a). The changes in $\delta^{53}Cr$ versus the UMIA values is shown in Figure 5(c). Two end members are present: one of the members is comprised of lateritic ores that have been enriched in lighter ^{52}Cr isotopes and which have a high index of alteration. The second member contains saprolitic ores with incipient alteration and Cr that has been enriched in heavy ^{53}Cr. When heavy and exchangeable Cr is removed, the remaining Cr is enriched in lighted isotopes thereby explaining

507 the negative $\delta^{53}Cr$ values of the lateritic ores. Conversely, when previously mobilized and
508 isotopically heavy Cr is once again deposited in saprolitic ores, this may lead to positive $\delta^{53}Cr$
509 values (Crowe et al., 2013; Frei and Polat, 2013; Berger and Frei, 2014).
510
511 The only geological reservoir that contains negative $\delta^{53}Cr$ is found in weathered rocks (Qin and
512 Wang, 2017). This was observed in the present study, except for the light isotope enrichment
513 found in the saprolitic ore samples (Figure 5(c)). A previous study found high $\delta^{53}Cr$ values in
514 serpentinites (up to +1.22‰) in response to serpentinization processes (Farkaš et al., 2013).
515 These authors interpreted the possible shift of altered peridotites to isotopically high $\delta^{53}Cr$ as
516 being due to less isotopically heavier Cr(VI) in serpentinizing fluids (Farkaš et al., 2013). It has
517 also been suggested higher $\delta^{53}Cr$ values occur in peridotite that has been altered and which is
518 characterized by lower Cr content (Wang et al., 2016). These authors offered two possible
519 explanations for this phenomenon: a) kinetic fractionation resulted in heavy Cr isotopes being
520 left behind when the fluids removed light Cr isotopes during the serpentinization process; or b)
521 fluids without isotopic fractionation first removed the light Cr isotopes and then isotopically heavy
522 Cr was accumulated during the reduction of sulfate, which occurred at a later stage. A third
523 explanation may also be the re-deposition of mobilized isotopically heavy Cr, along with the
524 enrichment of Cr (Crowe et al., 2013; Frei and Polat, 2013; Berger and Frei, 2014).
525
526 To assess this point, Figure 5(d) plots the isotopic signature of the total Cr against the
527 corresponding chemically extracted Cr(VI). The $\delta^{53}Cr$ values for the total Cr (+0.97 ± 0.08‰) and
528 the extracted Cr(VI) (+1.34 ± 0.07‰) contained in saprolitic ores are positive and are relatively
529 similar, suggesting that only minor losses of heavy Cr(VI) isotope occur in saprolitic ores. This
530 result is in line with the incipient degree of alteration of this material. Conversely, lateritic ores
531 display a considerably higher fractionation between total Cr (-0.76 ± 0.07‰) and Cr(VI)
532 (+4.37 ± 0.06‰). This is due to the loss of Cr(VI) that has been enriched in heavy isotopes
533 during weathering. Frei and Polat (2013) and Crowe et al. (2013) have stated that the oxidative
534 weathering of Cr is caused by the presence of oxygen in the atmosphere. As a result, runoff
535 removes the pool of ^{53}Cr-enriched Cr(VI) and the residual solid remains depleted in ^{53}Cr.
536
537 *5.3. Interactions between water and rocks during natural weathering*
538 The stream 1 is located outside of the mining area (Figure 1) and is used as a reference of the
539 natural processes at work in this ultramafic environment. The total dissolved Cr concentration in
540 stream 1 is much lower (0.1 µg L^{-1}) than the concentration determined in the bulk sample (8.7

μg L^{-1}). This suggests that the majority (over 98%) of the Cr found in the stream waters is contained in the SPM. Serpentinite soils are commonly comprised of a mixture of 90% solid Cr(III) oxy(hydr)oxides and 10% adsorbed Cr(VI). At pH values greater than 7, the runoff from these soils is dominated by dissolved Cr(VI) (Mcclain and Maher, 2016; Novak et al., 2017a; Coyte et al., 2020) that can therefore be released to the surface waters. Wu et al. (2017) studied samples collected in the Connecticut River (United States) fed by a watershed with high amounts of basalts and reported positive $\delta^{53}Cr$ values in the SPM. Most likely, one of the dominant factors controlling the weathering rates in watersheds is the lithology. Therefore, the weatherability of minerals decreases from carbonate > mafic silicates > feldspars > quartz (White and Blum, 1995). In the present study of the Barro Alto area, the $\delta^{53}Cr$ composition in the SPM (0.015 ± 0.09‰) collected in stream 1 and the inheritance of high amounts of $\delta^{53}Cr$ from dissolved Cr(VI) may be explained by the lithology (+2.60 ± 0.04‰).

The positive $\delta^{53}Cr$ values found in the dissolved fraction may either be the direct result of the Cr isotopic fractionation processes in an ultramafic profile, or they may be related to additional processes occurring during riverine transport such as redox fractionation processes, adsorption and/or mixing from riverine water with different $\delta^{53}Cr$ values (D'Arcy et al., 2016). It is also possible that the sorption of Cr(VI) onto Cr(III)-bearing oxy(hydr)oxides leads to decreased $\delta^{53}Cr$ values in the solid phase and discharged of the residual aqueous Cr(VI) into streams and rivers (Wang et al., 2015a). These scenarios seem less likely though, as the fractionation of Cr is less than 0.3‰ and there must be long-term contact between Cr(VI) and Cr(III) oxy(hydr)oxides (D'Arcy et al., 2016). The positive $\delta^{53}Cr$ values in stream 1 can be explained by the oxidation of Cr(III) to Cr(VI). However, it should be borne in mind that the large activation energy needed to carry out this transformation will not show a high fractionation (Zink et al., 2010). Wang et al. (2015a) evoked a "rind effect" to explain the low fractionation of solid Cr(III): Cr(III) oxy(hydr)oxide particles are comprised of several micro-layers, each of which is essentially completely oxidized, thereby resulting in limited isotopic fractionation. Stream 1 is characterized by both a large Cr isotopic fractionation and an elevated Fe concentration, consistent with processes dominated by the reduction of Cr(VI) into Cr(III), leaving ^{53}Cr-enriched Cr(VI) behind. It is also necessary to take into account the release of Cr(III) during weathering, as this may decrease the global amount of $\delta^{53}Cr$ present in the dissolved fraction (D'Arcy et al., 2016).

5.4. Mining activities resulting in accelerated weathering

When the ore is exploited in mines, a large amount of material must be removed and taken elsewhere. The scale of this operation is comparable to the effects of extensive physical erosion. Physical erosion has been described by White and Blum (1995) as one of several factors that control weathering rates. The concentrations of the SPM found in the water bodies inside the mine are significantly higher than the ones found in stream 1 (3.3-316 mg L^{-1} versus 1.1 mg L^{-1}, respectively). This shows unequivocally that the extraction, transport and stockpiling of the residues produced during mining activities results in the release of particles that find their way into sources of water. The analysis of the water bodies inside the mine showed that the SPM contains high concentrations of Cr (from 24 to 1064 µg L^{-1}). This enrichment in Cr could even be observed in the dissolved fraction (Cr concentrations < 757 µg L^{-1}). Wu et al. (2017) reported that there was no significant effect of oxide loads on the $\delta^{53}Cr$ values for the suspended Cr, particularly since the suspended Cr would have been isotopically heavy due to the inheritance of dissolved Cr(VI) $\delta^{53}Cr$ via adsorption. This result is in line with what we observed for the particulate Cr in stream 2, enriched in isotopically heavy Cr up to $\delta^{53}Cr$ value of +0.94 (± 0.09)‰), whereas the particulate Cr present in stream 1 remains unfractionated.

Material issued from the erosion of the overburden, waste rock, and extracted ores are released to the ponds via runoff water and as a result, these sediments are a mixture of various products. As observed in Figure 5(c), the negative $\delta^{53}Cr$ values determined for the sediments can be related to the enrichment in light isotopes of the lateritic ores (-0.76 (± 0.07)‰ to -0.16 (± 0.05)‰) and soils (-0.05 (± 0.04)‰ to -0.28 (± 0.06)‰). In pond 1, both Cr in the SPM and Cr in the sediments display negative isotopic signature (-0.38 (± 0.08)‰ and -0.50 (± 0.04)‰, respectively). The slightly higher values observed for Cr in sediments may be the result of the oxidation of Cr(III) as well as the release of Cr(VI) enriched in heavy isotopes. The basis of this hypothesis is that the sediments in the ponds are also a source of isotopically heavy Cr(VI) for the pond water column.

The groundwater sampled upstream and downstream from the smelter area shows enrichment in the total dissolved Cr (^{53}Cr equal to of +2.18 (± 0.08)‰ and +2.19 (± 0.16)‰, respectively; Figure 3). These values are in agreement with the range of $\delta^{53}Cr$ values (0.7 to 5.1‰) found by Izbicki et al. (2008) in 32 uncontaminated wells and by Coplen et al. (2002) in a study on native groundwater (1.1 to 5.8‰). In these samples, a significant fractionation occurs either on the mineral-grain surfaces or in bulk solutions when the dissolved oxygen concentrations decline and Cr is removed from solution as Cr(III) (Izbicki et al., 2008). Figure 3 shows that the depletion in heavy ^{53}Cr in the particulate fraction is higher before the smelter area than after (-

608 0.55 (± 0.06)‰ versus -0.34 (± 0.05)‰). Based on this result, it appears that the reductive
609 smelting process used on the ore to produce Fe-nickel (smelting at 1600°C) preferentially
610 liberates Cr(III) (Economou-Eliopoulos et al., 2016). When oxygen is depleted in the
611 groundwater, this can also lead to Cr(VI) being reduced to Cr(III) and, as a result, decreased
612 $\delta^{53}Cr$ values.
613
614 The isotopic signature of the Cr(VI) extracted was analyzed to determine how much of the Cr(VI)
615 found in the water bodies derived from the solid residues and ores. The $\delta^{53}Cr$ distribution for the
616 solids, extracted Cr(VI) and surface waters is given in Figure 6. The surface waters and
617 extracted Cr(VI) are characterized by variations within the same range, suggesting that surface
618 water and groundwater ^{53}Cr enrichment occurs as a result of the release of Cr(VI) oxidized from
619 Cr(III) in the solid phases. The natural weathering is partly contributing, while producing higher
620 Cr(VI) contents in more altered materials and, subsequently, ^{53}Cr depletion in the remaining
621 solid (Figure 6). Furthermore, a large contribution is directly related to anthropically enhanced
622 erosion caused by mining activities, which accelerates natural weathering processes.
623
624 **6. Conclusions**

625 This study is an important step towards improving our understanding of Cr isotope behavior in
626 ultramafic environments and more specifically in mining areas. The reconstructed pedological
627 profile combined with the results of the UMIA (ultramafic index of alteration) shows that the
628 lateritic ores and soils were subjected to an intense mineralogical transformation. They are
629 enriched in both Cr (10-18 g kg^{-1}) and Fe (85-536 g kg^{-1}) and the exchangeable pool of Cr(VI)
630 ($E_{Cr(VI)}$) also becomes larger with increasing degrees of alteration.
631
632 The analyses performed on the saprolitic ores suggest that very small amounts of heavy Cr(VI)
633 are lost as attested by the positive $\delta^{53}Cr$ values total Cr (+0.97 (± 0.08‰) and extracted Cr(VI)
634 (+1.34 (± 0.07)‰) as well as the close similarity between the values. Conversely, there is a
635 considerably larger difference between the fractionation of the total Cr (-0.76 (± 0.07)‰) and the
636 extracted Cr(VI) (+4.37 (± 0.06)‰) observed in the lateritic ores as a result of the loss/leaching
637 of isotopically heavy and exchangeable Cr(VI) during weathering. Consequently, negatively
638 fractionated Cr is left behind.
639
640 Our study shows that ^{53}Cr enrichment in both the surface water and groundwater is related to
641 the release of Cr(VI) due to the Cr(III) oxidation in the solid phases. This is demonstrated by

comparing the range of variation of $\delta^{53}Cr$ between the surface waters and the extracted Cr(VI). The former (+2.10 (± 0.04) to +3.66 (± 0.04) ‰) falls within the range of the latter (+1.34 (± 0.07) to +4.37 (± 0.06) ‰). Some of the enrichment in Cr is due to natural weathering, however, erosion due to mining activities is playing an important role as this accelerates natural weathering. In our study, the pristine area is represented by stream 1 which has lower total Cr concentrations than the other surface waters evaluated. Nevertheless, it should be noted that the $\delta^{53}Cr$ value still falls within the range of variation for the extracted Cr(VI). It may be possible to use $\delta^{53}Cr$ values to trace sources of Cr in the dissolved fraction, assuming the combination of this tool with other parameters such as total Cr, Fe and Mn concentration, organic carbon and, most of all, Cr speciation to obtain the full picture and to accurately interpret these data.

Acknowledgements

The authors would like to thank Anglo American for access to their field facilities and for releasing samples. We would also like to thank the Anglo American staff for their help during the sampling campaign. Sincere thanks go to Dr. Sophie Nowak for performing the XRD acquisition in the RX platform in the Paris Diderot Chemistry Department. The authors thank the European Commission (EC) for providing financial support via the Erasmus Mundus Joint Doctorate Program ETeCoS^3 (Environmental Technologies for Contaminated Solids, Soils and Sediments, grant agreement FPA no 2010-0009). This work was carried out as part of the Marie Curie International Research Staff Exchange Scheme Fellowship within the seventh European Community Framework Program (NIDYFICS, n°318123). Some of this work was supported by the IPGP multidisciplinary program PARI, and by Paris–IdF region SESAME Grant no. 12015908. This work was also supported by the CNPq (Conselho Nacional de Desenvolvimento Científico e Tecnológico, Brazil) under contract N° 445423/2014-5, 420697/2018-7 and 302722/2018-1.

7. References

Aiglsperger, T., Proenza, J.A., Lewis, J.F., Labrador, M., Svojtka, M., Rojas-purón, A., Longo, F., Jana, Ď., 2016. Critical metals (REE, Sc, PGE) in Ni laterites from Cuba and the Dominican Republic. Ore Geol. Rev. 73, 127–147. https://doi.org/10.1016/j.oregeorev.2015.10.010

Becquer, T., Quantin, C., Boudot, J.P., 2010. Toxic levels of metals in Ferralsols under natural vegetation and crops in New Caledonia. Eur. J. Soil Sci. 61, 994–1004.

674 Becquer, T., Quantin, C., Rotte-Capet, S., Ghanbaja, J., Mustin, C., Herbillon, A.J., 2006.
675 Sources of trace metals in Ferralsols in New Caledonia. Eur. J. Soil Sci. 57, 200–213.

676 Becquer, T., Quantin, C., Sicot, M., Boudot, J.P., 2003. Chromium availability in ultramafic soils
677 from New Caledonia. Sci. Total Environ. 301, 251–261. https://doi.org/10.1016/S0048-
678 9697(02)00298-X

679 Berger, A., Frei, R., 2014. The fate of chromium during tropical weathering: A laterite profile from
680 central madagascar. Geoderma 213, 521–532.
681 https://doi.org/10.1016/j.geoderma.2013.09.004

682 Birck, J.L., Allegre, C.J., 1988. Manganese-chromium isotope systematics and the development
683 of the early Solar System. Nature 331, 579–584.

684 Bolaños-Benítez, V., van Hullebusch, E.D., Garnier, J., Quantin, C., Tharaud, M., Lens, P.N.L.,
685 Sivry, Y., 2018. Assessing chromium mobility in natural surface waters: Colloidal
686 contribution to the isotopically exchangeable pool of chromium (EwCrvalue). Appl.
687 Geochemistry 92, 19–29. https://doi.org/10.1016/j.apgeochem.2018.02.007

688 Coleman, R.G., Jove, C., 1993. Geological origin of serpentinites, in: The Vegetation of
689 Ultramafic (Serpentine) Soils. Andover, NH, pp. 1–17.

690 Coplen, T.B., Hopple, J. a, Böhlke, J.K., Peiser, H.S., Rieder, S.E., Krouse, H.R., Rosman,
691 K.J.R., Ding, T., Vocke, R.D.J., Révész, K.M., Lamberty, a, Taylor, P., Bièvre, P. De, 2002.
692 Compilation of minimum and maximum isotope ratios of selected elements in naturally
693 occurring terrestrial materials and reagents. Usgs 110.

694 Coyte, R.M., Mckinley, K.L., Jiang, S., Karr, J., Dwyer, G.S., Keyworth, A.J., Davis, C.C.,
695 Kondash, A.J., Vengosh, A., 2020. Occurrence and distribution of hexavalent chromium in
696 groundwater. Sci. Total Environ. 711, 135–135.
697 https://doi.org/10.1016/j.scitotenv.2019.135135

698 Crowe, S.A., Døssing, L.N., Beukes, N.J., Bau, M., Kruger, S.J., Frei, R., Canfield, D.E., 2013.
699 Atmospheric oxygenation three billion years ago. Nature 501, 535–538.
700 https://doi.org/10.1038/nature12426

701 D'Arcy, J., Babechuk, M.G., Døssing, L.N., Gaucher, C., Frei, R., 2016. Processes controlling
702 the chromium isotopic composition of river water: Constrains from basaltic river catchments.

703 Geochim. Cosmochim. Acta 186, 296–315. https://doi.org/10.1016/j.gca.2016.04.027

704 Economou-Eliopoulos, M., Frei, R., Megremi, I., 2016. Potential leaching of Cr (VI) from laterite
705 mines and residues of metallurgical products (red mud and slag): An integrated approach.
706 J. Geochemical Explor. 162, 40–49. https://doi.org/10.1016/j.gexplo.2015.12.007

707 Ellis, A.S., Johnson, T.M., Bullen, T.D., 2002. Chromium Isotopes and the Fate of Hexavalent
708 Chromium in the Environment. Science. 295, 2060–2062.
709 https://doi.org/10.1126/science.1068368

710 Fandeur, D., Juillot, F., Morin, G., Livi, L., Cognigni, A., Webb, S.M., Ambrosi, J.P., Fritsch, E.,
711 Guyot, F., Brown, G.E., 2009. XANES evidence for oxidation of Cr(III) to Cr(VI) by Mn-
712 oxides in a lateritic regolith developed on serpentinized ultramafic rocks of New Caledonia.
713 Environ. Sci. Technol. 43, 7384–7390. https://doi.org/10.1021/es900498r

714 Farkaš, J., Chrastný, V., Novák, M., Čadkova, E., Pašava, J., Chakrabarti, R., Jacobsen, S.B.,
715 Ackerman, L., Bullen, T.D., 2013. Chromium isotope variations (δ53/52Cr) in mantle-
716 derived sources and their weathering products: Implications for environmental studies and
717 the evolution of δ53/52Cr in the Earth's mantle over geologic time. Geochim. Cosmochim.
718 Acta 123, 74–92. https://doi.org/10.1016/j.gca.2013.08.016

719 Fendorf, S.E., 1995. Surface reactions of chromium in soils and waters. Geoderma 67, 55–71.
720 https://doi.org/10.1016/0016-7061(94)00062-F

721 Fendorf, S.E., Zasoski, R.J., 1992. Chromium(Iii) Oxidation By Delta-Mno2 .1. Characterization.
722 Environ. Sci. Technol. 26, 79–85.

723 Ferreirafilho, C., Nilson, a, Naldrett, a, 1992. The Niquelândia Mafic-Ultramafic Complex,
724 Goias, Brazil: a contribution to the ophiolite X stratiform controversy based on new
725 geological and structural data. Precambrian Res. 59, 125–143.
726 https://doi.org/10.1016/0301-9268(92)90054-R

727 Frei, R., Polat, A., 2013. Chromium isotope fractionation during oxidative weathering-
728 implications from the study of a Paleoproterozoic (ca. 1.9 Ga) paleosol, Schreiber Beach,
729 Ontario, Canada. Precambrian Res. 224, 434–453.
730 https://doi.org/10.1016/j.precamres.2012.10.008

731 Garnier, J., Quantin, C., Echevarria, G., Becquer, T., 2009a. Assessing chromate availability in

732 tropical ultramafic soils using isotopic exchange kinetics. J. Soils Sediments 9, 468–475.
733 https://doi.org/10.1007/s11368-009-0062-4

734 Garnier, J., Quantin, C., Guimaraes, E., Becquer, T., 2008. Can chromite weathering be a
735 source of Cr in soils? Mineral. Mag. 72, 49–53.

736 Garnier, J., Quantin, C., Guimarães, E., Garg, V.K., Martins, E.S., Becquer, T., 2009b.
737 Understanding the genesis of ultramafic soils and catena dynamics in Niquelândia, Brazil.
738 Geoderma 151, 204–214. https://doi.org/10.1016/j.geoderma.2009.04.020

739 Garnier, J., Quantin, C., Guimarães, E.M., Vantelon, D., Montargès-Pelletier, E., Becquer, T.,
740 2013. Cr(VI) genesis and dynamics in Ferralsols developed from ultramafic rocks: The case
741 of Niquelândia, Brazil. Geoderma 193–194, 256–264.
742 https://doi.org/10.1016/j.geoderma.2012.08.031

743 Garnier, J., Quantin, C., Martins, E.S., Becquer, T., 2006. Solid speciation and availability of
744 chromium in ultramafic soils from Niquelândia, Brazil. J. Geochemical Explor. 88, 206–209.
745 https://doi.org/10.1016/j.gexplo.2005.08.040

746 Izbicki, J. a., Ball, J.W., Bullen, T.D., Sutley, S.J., 2008. Chromium, chromium isotopes and
747 selected trace elements, western Mojave Desert, USA. Appl. Geochemistry 23, 1325–1352.
748 https://doi.org/10.1016/j.apgeochem.2007.11.015

749 Leita, L., Margon, A., Pastrello, A., Arčon, I., Contin, M., Mosetti, D., 2009. Soil humic acids may
750 favour the persistence of hexavalent chromium in soil. Environ. Pollut. 157, 1862–1866.
751 https://doi.org/10.1016/j.envpol.2009.01.020

752 Lombi, E., Hamon, R.E., Mcgrath, S.P., Mclaughlin, M.J., 2003. Lability of Cd, Cu, and Zn in
753 Polluted Soils Treated with Lime, Beringite, and Red Mud and Identification of a Non-Labile
754 Colloidal Fraction of Metals Using Isotopic Techniques. Environ. Sci. Technol. 37, 979–984.

755 Losfeld, G., Huillier, L.L., Fogliani, B., Jaffré, T., 2014. Mining in New Caledonia: environmental
756 stakes and restoration opportunities. Environ. Sci. Pollut. Res. 22, 5592–5607.
757 https://doi.org/10.1007/s11356-014-3358-x

758 Marzouk, E.R., Chenery, S.R., Young, S.D., 2013. Measuring reactive metal in soil : a
759 comparison of multi-element isotopic dilution and chemical extraction. Eur. J. Soil Sci. 64,
760 526–536. https://doi.org/10.1111/ejss.12043

761 Mcclain, C.N., Maher, K., 2016. Chromium fl uxes and speciation in ultrama fi c catchments and
762 global rivers. Chem. Geol. 426, 135–157. https://doi.org/10.1016/j.chemgeo.2016.01.021

763 Moore, P., 2012. Anglo's new nickel, International mining. 20-24

764 Novak, M., Chrastny, V., Cadkova, E., Farkas, J., Bullen, T.D., Tylcer, J., Szurmanova, Z., Cron,
765 M., Prechova, E., Curik, J., Stepanova, M., Pasava, J., Erbanova, L., Houskova, M.,
766 Puncochar, K., Hellerich, L.A., 2014. Common occurrence of a positive δ53Cr shift in
767 central european waters contaminated by geogenic/industrial chromium relative to source
768 values. Environ. Sci. Technol. 48, 6089–6096. https://doi.org/10.1021/es405615h

769 Novak, M., Chrastny, V., Sebek, O., Martinkova, E., Prechova, E., Curik, J., Veselovsky, F.,
770 Stepanova, M., Dousova, B., Buzek, F., Farkas, J., Andronikov, A., Cimova, N., Houskova,
771 M., 2017a. Chromium isotope fractionations resulting from electroplating, chromating and
772 anodizing: Implications for groundwater pollution studies. Appl. Geochemistry 80, 134–142.
773 https://doi.org/10.1016/j.apgeochem.2017.03.009

774 Novak, M., Kram, P., Sebek, O., Andronikov, A., Chrastny, V., Martinkova, E., Stepanova, M.,
775 Prechova, E., Curik, J., Veselovsky, F., Myska, O., Stedra, V., Farkas, J., 2017b. Temporal
776 changes in Cr fluxes and δ53Cr values in runoff from a small serpentinite catchment
777 (Slavkov Forest, Czech Republic). Chem. Geol. 472, 22–30.
778 https://doi.org/10.1016/j.chemgeo.2017.09.023

779 Oze, C., Fendorf, S., Bird, D.K., Coleman, R.G., 2004. Chromium Geochemistry of Serpentine
780 Soils. Int. Geol. Rev. 46, 97–126. https://doi.org/10.2747/0020-6814.46.2.97

781 Paulukat, C., Døssing, L.N., Mondal, S.K., Voegelin, A.R., Frei, R., 2015. Oxidative release of
782 chromium from Archean ultramafic rocks, its transport and environmental impact – A Cr
783 isotope perspective on the Sukinda valley ore district (Orissa, India). Appl. Geochemistry
784 59, 125–138. https://doi.org/10.1016/j.apgeochem.2015.04.016

785 Qin, L., Wang, X., 2017. Chromium Isotope Geochemistry. Rev. Mineral. Geochemistry 82, 379–
786 414.

787 Rai, D., Eary, L.E., Zachara, J.M., 1989. Environmental chemistry of chromium. Sci. Total
788 Environ. 86, 15–23.

789 Raous, S., Becquer, T., Garnier, J., Martins, É.D.S., Echevarria, G., Sterckeman, T., 2010.

790 Mobility of metals in nickel mine spoil materials. Appl. Geochemistry 25, 1746–1755.
791 https://doi.org/10.1016/j.apgeochem.2010.09.001

792 Raous, S., Echevarria, G., Sterckeman, T., Hanna, K., Thomas, F., Martins, E.S., Becquer, T.,
793 2013. Potentially toxic metals in ultramafic mining materials: Identification of the main
794 bearing and reactive phases. Geoderma 192, 111–119.
795 https://doi.org/10.1016/j.geoderma.2012.08.017

796 Ratié, G., Garnier, J., Calmels, D., Vantelon, D., Guimaraes, E., Monvoisin, G., Nouet, J.,
797 Ponzevera, E., Quantin, C., 2018. Nickel distribution and isotopic fractionation in a Brazilian
798 lateritic regolith: Coupling Ni isotopes and Ni K-edge XANES. Geochim. Cosmochim. Acta
799 230, 137–154. https://doi.org/10.1016/j.gca.2018.03.026

800 Ratié, G., Jouvin, D., Garnier, J., Rouxel, O., Miska, S., Guimarães, E., Vieira, L.C., Sivry, Y.,
801 Zelano, I., Pelletier, E.M., Thil, F., Quantin, C., 2015. Nickel isotope fractionation during
802 tropical weathering of ultrama fi c rocks. Chem. Geol. 402, 68–76.
803 https://doi.org/10.1016/j.chemgeo.2015.02.039

804 Ratié, G., Quantin, C., Jouvin, D., Calmels, D., Ettler, V., Sivry, Y., Vieira, L.C., Ponzevera, E.,
805 Garnier, J., 2016. Nickel isotope fractionation during laterite Ni ore smelting and refining:
806 Implications for tracing the sources of Ni in smelter-affected soils. Appl. Geochemistry 64,
807 136–145. https://doi.org/10.1016/j.apgeochem.2015.09.005

808 Rivera, J., Reich, M., Schoenberg, R., González-jiménez, J.M., Barra, F., Aiglsperger, T.,
809 Proenza, J.A., Carretier, S., 2018. Platinum-group element and gold enrichment in soils
810 monitored by chromium stable isotopes during weathering of ultramafic rocks. Chem. Geol.
811 499, 84–99. https://doi.org/10.1016/j.chemgeo.2018.09.008

812 Schauble, E., Rossman, G.R., Taylor, H.P., 2004. Theoretical estimates of equilibrium
813 chromium-isotope fractionations 205, 99–114.
814 https://doi.org/10.1016/j.chemgeo.2003.12.015

815 Trebien, D.O.P., Bortolon, L., Tedesco, M.J., Bissani, C.A., Camargo, F.A.O., 2011.
816 Environmental Factors Affecting Chromium-Manganese Oxidation-Reduction Reactions in
817 Soil. Pedosphere 21, 84–89.

818 Trinquier, A., Birck, J.-L., Allègre, C.J., 2008. High-precision analysis of chromium isotopes in
819 terrestrial and meteorite samples by thermal ionization mass spectrometry. J. Anal. At.

820 Spectrom. 23, 1565. https://doi.org/10.1039/b809755k

821 Vithanage, M., Kumarathilaka, P., Oze, C., Karunatilake, S., 2019. Occurrence and cycling of
822 trace elements in ultramafic soils and their impacts on human health: A critical review.
823 Environ. Int. 131, 104974. https://doi.org/10.1016/j.envint.2019.104974

824 Vojcu, G., Bardoux, M., 1997. Mineralogical norm calculations applied tropical weathering
825 profiles. Mineral. Mag. 61, 185–196.

826 Wang, X., Johnson, T.M., Ellis, A.S., 2015a. Equilibrium isotopic fractionation and isotopic
827 exchange kinetics between Cr(III) and Cr(VI). Geochim. Cosmochim. Acta 153, 72–90.
828 https://doi.org/10.1016/j.gca.2015.01.003

829 Wang, X., Johnson, T.M., Ellis, A.S., 2015b. Equilibrium isotopic fractionation and isotopic
830 exchange kinetics between Cr(III) and Cr(VI). Geochim. Cosmochim. Acta 153, 72–90.
831 https://doi.org/10.1016/j.gca.2015.01.003

832 Wang, X., Planavsky, N.J., Reinhard, C.T., Zou, H., Ague, J.J., Wu, Y., Gill, B.C.,
833 Schwarzenbach, E.M., Peucker-Ehrenbrink, B., 2016. Chromium isotope fractionation
834 during subduction-related metamorphism, black shale weathering, and hydrothermal
835 alteration. Chem. Geol. 423, 19–33. https://doi.org/10.1016/j.chemgeo.2016.01.003

836 White, A.F., Blum, A.E., 1995. Effects of climate on chemical weathering in watersheds.
837 Geochim. Cosmochim. Acta 59, 1729–1747. https://doi.org/10.1016/0016-7037(95)00078-E

838 Wu, W., Wang, X., Reinhard, C.T., Planavsky, N.J., 2017. Chromium isotope systematics in the
839 Connecticut River. Chem. Geol. 456, 98–111.
840 https://doi.org/10.1016/j.chemgeo.2017.03.009

841 Zachara, J.M., Ainsworth, C.C., Cowan, C.E., Resch, C.T., 1989. Adsorption of Chromate by
842 Subsurface Soil Horizons, Soil Science Society of America Journal - SSSAJ.
843 https://doi.org/10.2136/sssaj1989.03615995005300020018x

844 Zelano, I., Sivry, Y., Quantin, C., Gélabert, A., Tharaud, M., Nowak, S., Garnier, J., Malandrino,
845 M., Benedetti, M.F., 2016. Study of Ni exchangeable pool speciation in ultramafic and
846 mining environments with isotopic exchange kinetic data and models. Appl. Geochemistry
847 64, 146–156. https://doi.org/10.1016/j.apgeochem.2015.09.021

848 Zink, S., Schoenberg, R., Staubwasser, M., 2010. Isotopic fractionation and reaction kinetics

between Cr(III) and Cr(VI) in aqueous media. Geochim. Cosmochim. Acta 74, 5729–5745. https://doi.org/10.1016/j.gca.2010.07.015

Figure 1. Map of the study area in Barro Alto mine and location of the sampling sites. Names in parenthesis are the ones used for the solid samples.

Figure 2. Positive correlation between isotopically and chemically exchangeable pool of Cr(VI) in solid samples of Barro Alto.

Figure 3. Cr isotopic composition in ‰ of the samples from this study, including solid samples (soils, ores, bedrock and sediments), Cr(VI) extracted with KH_2PO_4 and liquid samples (surface and ground water).

Figure 4. Ternary plot in the Al-Fe-Mg-Si space and its relationship with the ultramafic index of alteration (UMIA).

Figure 5. Evolution, according to the ultramafic index of alteration of a) the total Cr content, b) the exchangeable pool of Cr, c) the Cr isotopic composition of the bulk samples and d) the Cr isotopic composition of both bulk samples and corresponding extracted Cr(VI) (KH_2PO_4).

Figure 6. Total chromium contents in solid samples and their correspondent $\delta^{53}Cr$ values. The blue band represents the $\delta^{53}Cr$ range of variation in surface water, which is within the range found for Cr(VI) extracted with KH_2PO_4.

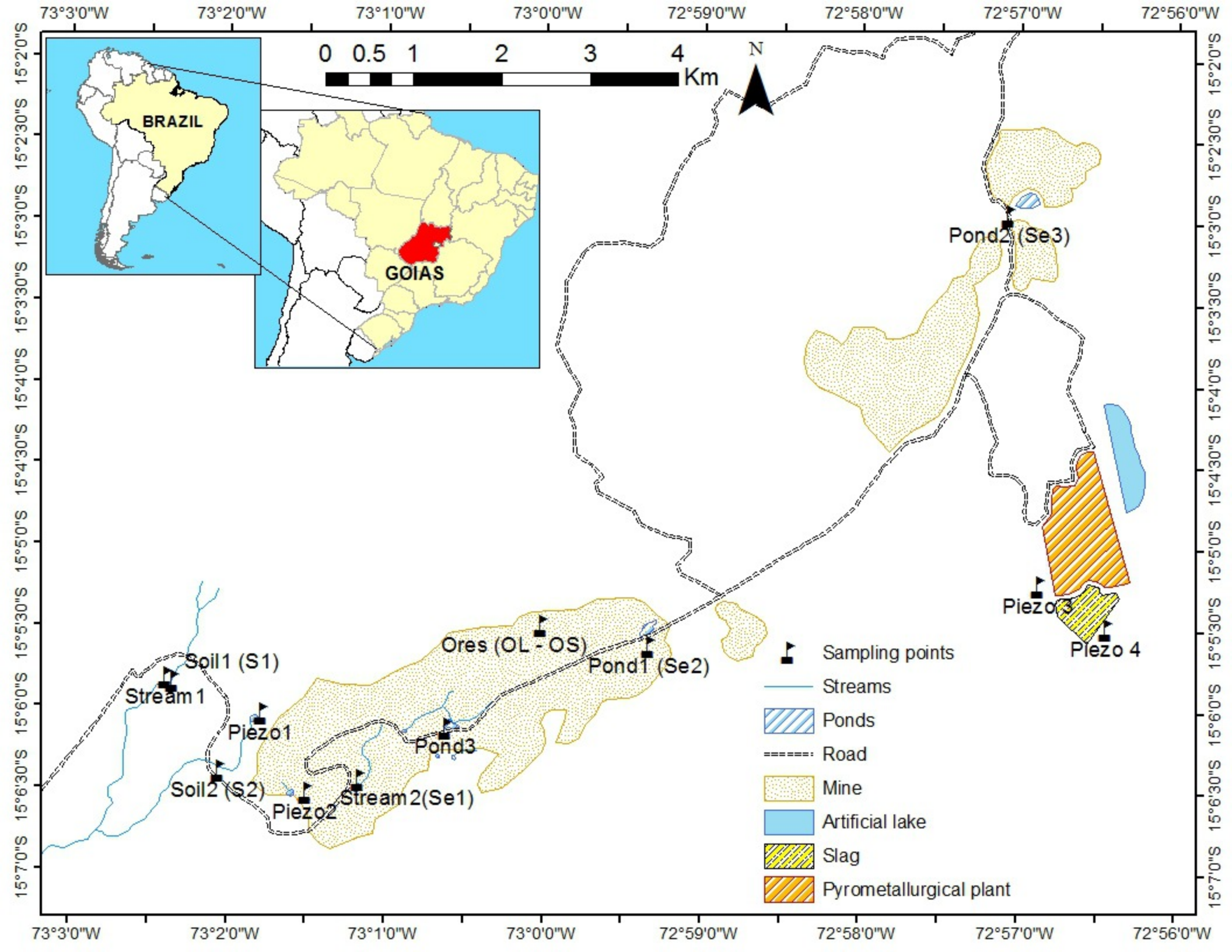
BRAZIL
GOIAS
0 0.5 1 2 3 4
Km
N
Pond2 (Se3)
Piezo 3
Piezo 4
Ores (OL - OS)
Pond1 (Se2)
Soil1 (S1)
Stream1
Piezo1
Pond3
Soil2 (S2)
Piezo2
Stream2(Se1)
Sampling points
Streams
Ponds
Road
Mine
Artificial lake
Slag
Pyrometallurgical plant
73°3'0"W
73°2'0"W
73°1'0"W
73°0'0"W
72°59'0"W
72°58'0"W
72°57'0"W
72°56'0"W
15°2'0"S
15°2'30"S
15°3'0"S
15°3'30"S
15°4'0"S
15°4'30"S
15°5'0"S
15°5'30"S
15°6'0"S
15°6'30"S
15°7'0"S

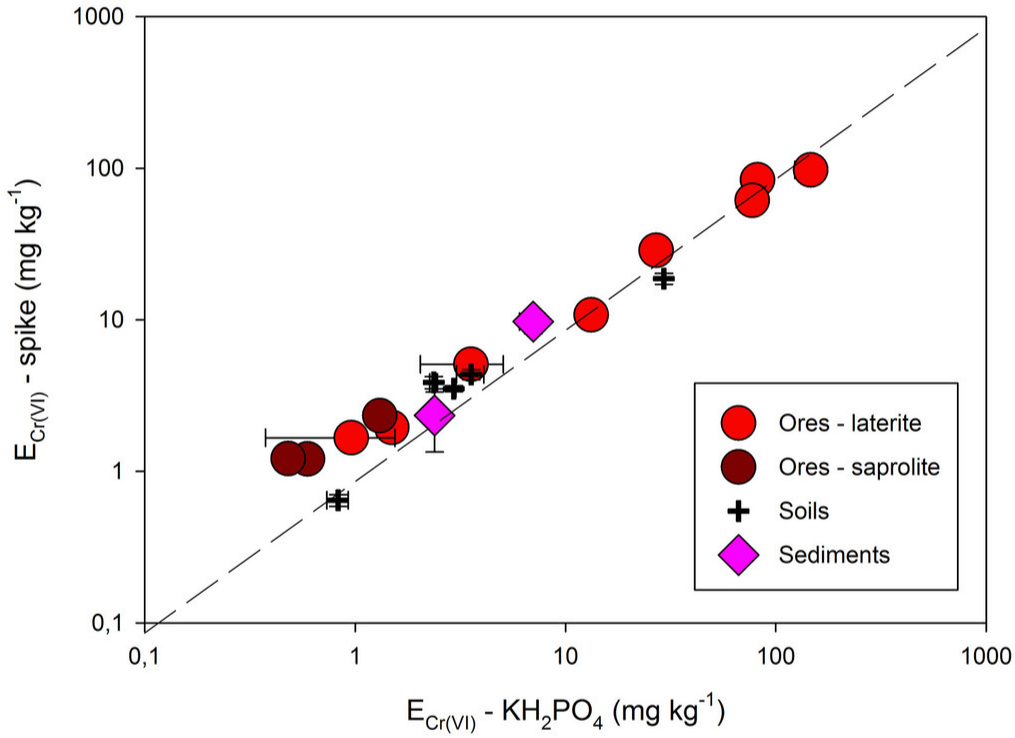
1000
100
10
1
0,1
0,1
1
10
100
1000
$E_{Cr(VI)}$ - spike (mg kg^{-1})
$E_{Cr(VI)}$ - KH_2PO_4 (mg kg^{-1})
Ores - laterite
Ores - saprolite
Soils
Sediments

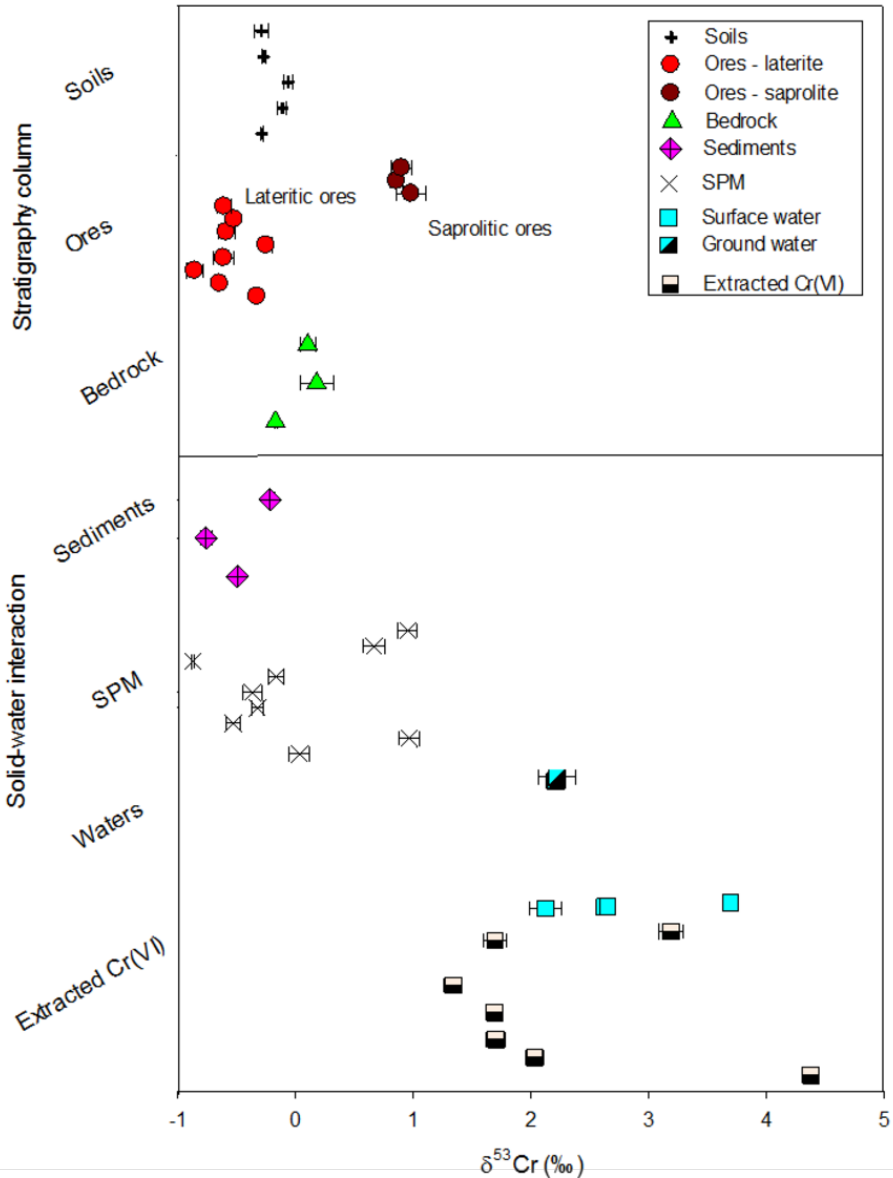
Stratigraphy column
Soils
Ores
Bedrock
Lateritic ores
Saprolitic ores
Soils
Ores - laterite
Ores - saprolite
Bedrock
Sediments
SPM
Surface water
Ground water
Extracted Cr(VI)
Solid-water interaction
Sediments
SPM
Waters
Extracted Cr(VI)
-1
0
1
2
3
4
5
δ53Cr (‰)

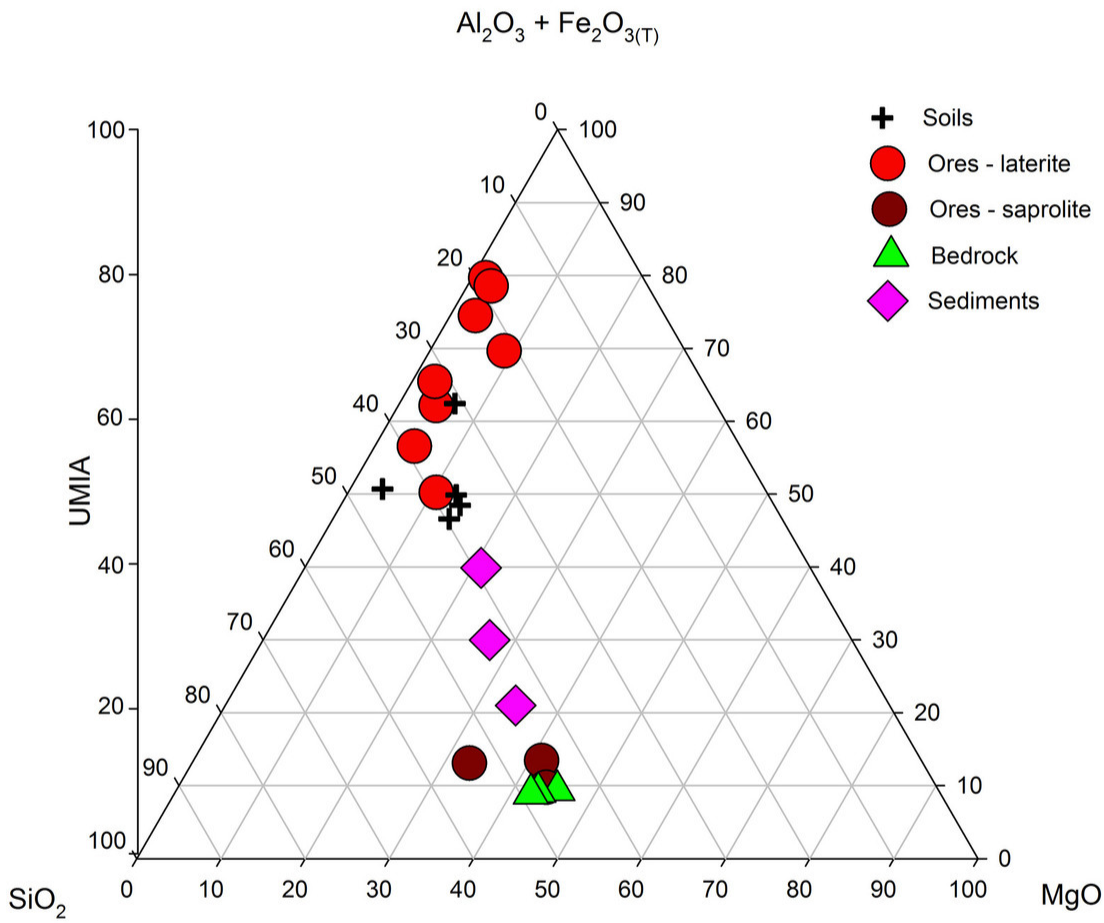
$Al_2O_3 + Fe_2O_{3(T)}$
UMIA
SiO_2
MgO
Soils
Ores - laterite
Ores - saprolite
Bedrock
Sediments

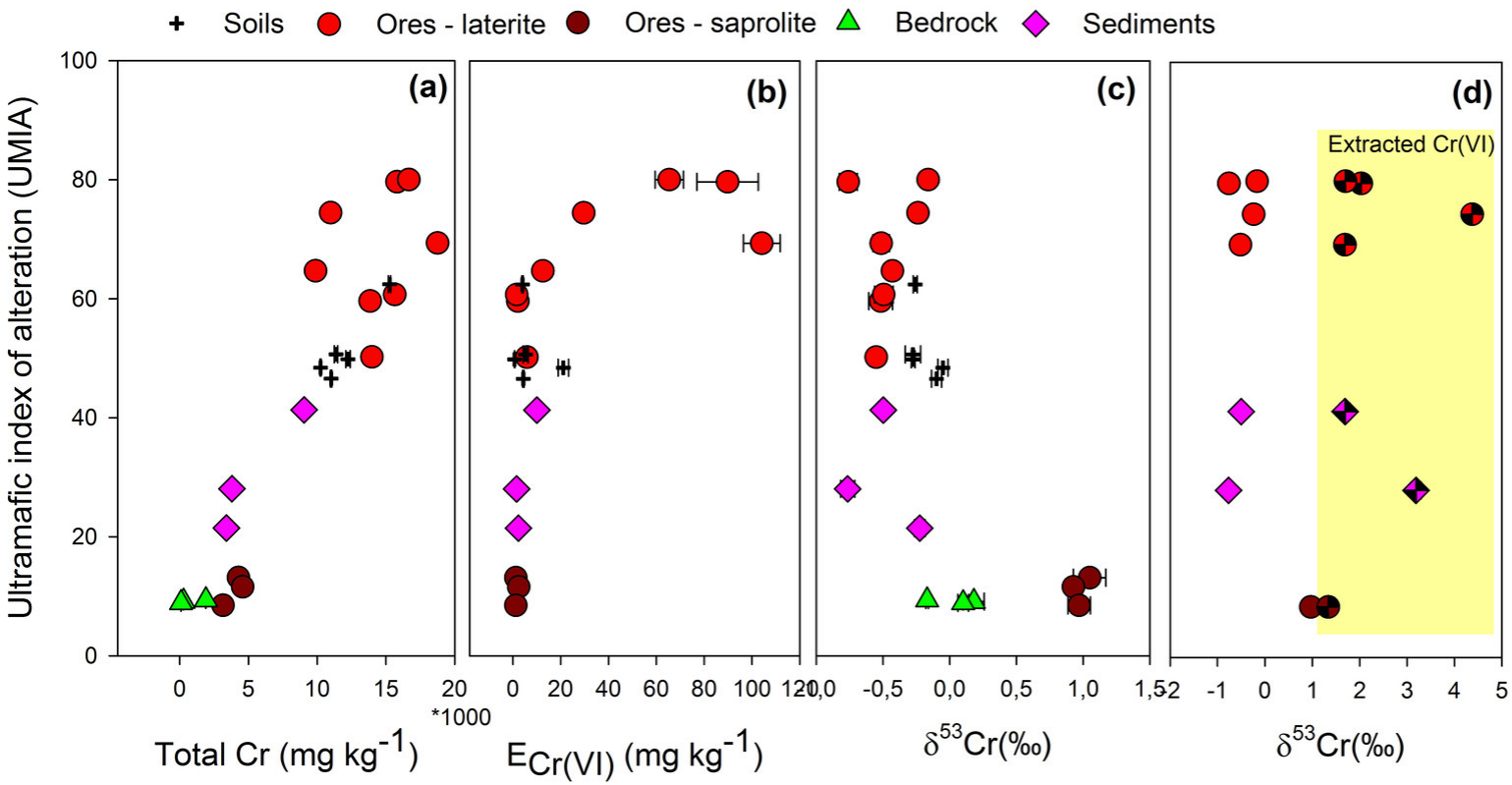
Soils
Ores - laterite
Ores - saprolite
Bedrock
Sediments
(a)
(b)
(c)
(d)
Extracted Cr(VI)
Ultramafic index of alteration (UMIA)
Total Cr (mg kg-1)
*1000
ECr(VI) (mg kg-1)
δ53Cr(‰)
δ53Cr(‰)

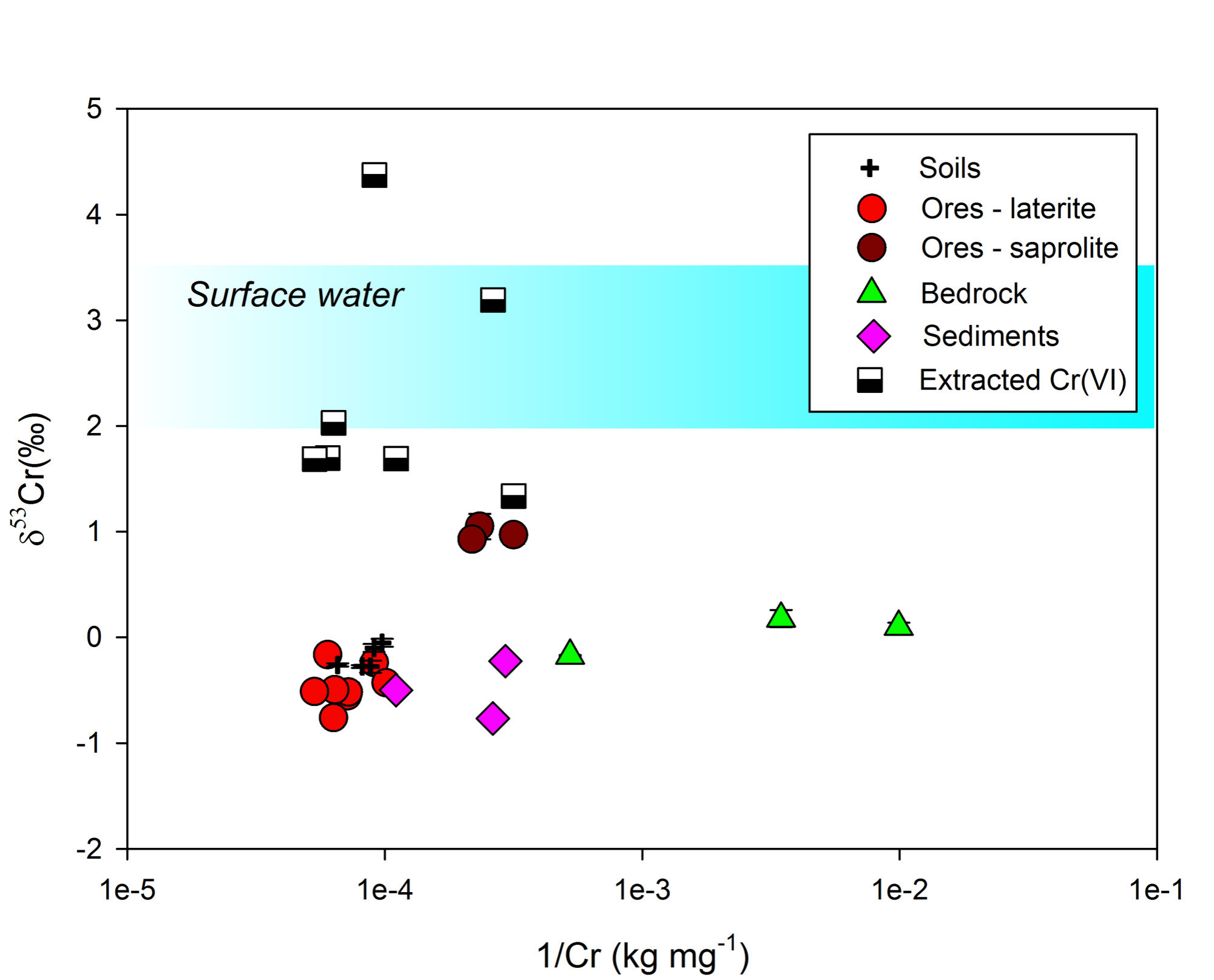
Surface water
Soils
Ores - laterite
Ores - saprolite
Bedrock
Sediments
Extracted Cr(VI)
δ53Cr(‰)
1/Cr (kg mg-1)
5
4
3
2
1
0
-1
-2
1e-5
1e-4
1e-3
1e-2
1e-1

Table 1 Total content of elements, $\delta^{53}Cr$ value and mineralogical composition of the solids collected in Barro Alto (soils, ores, bedrock and sediments). Sm: smectite; Srp: serpentine; Chl: chlorite; talc, Oli: olivine; Hem: hematite; Goe: goethite; Spi: Spinel and Qz: quartz (n.d. = not determined). τ represent the enrichment or depletion of Cr respect to the bedrock. UMIA is the Ultramafic Index of Alteration (Aiglsperger et al., 2016).

Sample type	Sample code	τ Cr/Ti	UMIA	$\delta^{53}Cr$ (‰)	±2σ	Concentration (g kg^{-1})								Mineralogy							
						Si	Al	Cr	Fe	Mg	Mn	Ni	Ti	Sm	Srp	Chl	Talc	Oli	Hem	Goe	Spi	Qz	Others
Soils	S1(0-10 cm)	0.19	50	-0.28	0.01	97.28	76.97	12.23	280.71	34.51	4.04	6.68	1.24			+			+			+	
	S1(10-40 cm)	0.25	47	-0.10	0.04	107.96	74.29	11.01	250.13	38.16	3.75	6.45	1.06			+			+			+	
	S1(80-100 cm)	0.06	48	-0.05	0.04	101.08	79.47	10.24	271.35	35.96	3.02	6.12	1.16			+	+		+				
	S2(0-15 cm)	0.88	62	-0.26	0.01	69.47	76.62	15.26	330.05	15.96	10.69	8.75	0.98			+	+		+	+		+	Magnetite
	S2(15-40 cm)	0.83	51	-0.28	0.06	109.55	62.44	11.37	272.25	11.67	9.98	6.47	0.75						+	+		+	Chromite
Lateritic ores	OL1	1.06	74	-0.24	0.02	27.33	48.43	10.97	331.82	10.92	3.92	8.08	0.64							+	+	+	
	OL2	3.60	50	-0.55	0.03	60.59	30.56	13.98	369.02	32.74	5.85	21.73	0.37	+	+					+			
	OL3	1.83	80	-0.76	0.07	20.82	42.13	15.80	536.17	9.14	6.92	3.90	0.67			+			+	+	+	+	
	OL4	1.09	60	-0.52	0.09	51.54	69.72	13.85	424.30	21.54	6.27	22.19	0.80							+			
	OL5	0.97	80	-0.16	0.05	19.59	66.91	16.65	465.59	15.59	7.05	12.23	1.02							+			
	OL6	1.91	61	-0.50	0.07	46.75	57.97	15.64	403.85	24.52	6.22	21.10	0.65		+					+			
	OL7	1.15	65	-0.43	0.02	42.65	42.02	9.88	297.78	13.80	4.66	10.05	0.55	+						+			
	OL8	1.52	69	-0.51	0.06	26.47	63.13	18.75	451.98	24.80	6.49	15.35	0.89							+	+		
Saprolitic ores	OS1	1.38	13	1.05	0.12	167.68	17.89	4.28	109.58	105.95	2.47	31.51	0.22		+								Vermiculite
	OS2	0.93	12	0.93	0.05	158.76	15.78	4.58	133.78	156.44	2.40	22.16	0.29	+	+								
	OS3	1.45	8	0.97	0.08	179.15	13.84	3.16	84.93	146.54	1.03	21.56	0.16	+	+								
Bedrock	B1	-	10	-0.17	0.01	n.d.	0.60	0.27	103.34	202.23	0.20	1.00	n.d.		+								Chromite
	B2	-	11	0.18	0.08	188.00	1.59	1.23	22.40	182.70	1.01	2.67	0.10		+	+		+					Amphibole
	B3	-	11	0.10	0.04	194.00	0.79	1.33	22.40	156.20	1.01	2.75	0.21		+	+		+				+	
Sediments	Se1	-0.65	28	-0.77	0.05	145.65	20.50	3.81	264.19	65.87	3.30	16.84	1.30		+	+				+		+	
	Se2	1.28	41	-0.50	0.04	108.53	43.65	9.05	331.93	48.54	3.79	8.85	0.48			+					+	+	
	Se3	-0.41	21	-0.23	0.04	162.24	11.43	3.40	201.81	86.14	2.82	12.97	0.70		+	+			+				

* n.d.= not determined

Table 2 Exchangeable pool of Cr(VI) ($E_{Cr(VI)}$-KH_2PO_4) and Cr(III) ($E_{Cr(III)}$-KCl) in the solid samples.

Sample type	Sample code	$E_{Cr(VI)}$-KH_2PO_4 (mg kg^{-1})	SD	$E_{Cr(III)}$-KCl (mg kg^{-1})	SD
Soils	S1(0-10 cm)	0.74	0.06	<LoD	-
	S1(10-40 cm)	4.43	0.34	0.39	0.02
	S1(80-100 cm)	21.14	2.17	3.69	0.54
	S2(0-15 cm)	4.06	0.30	0.34	0.03
	S2(15-40 cm)	5.39	1.05	0.43	0.01
Lateritic ores	OL1	29.65	2.64	7.49	0.43
	OL2	5.84	0.68	0.57	0.05
	OL3	89.79	1.82	7.30	0.30
	OL4	2.04	0.25	0.25	0.02
	OL5	65.44	5.96	10.46	0.38
	OL6	1.68	0.16	0.20	0.03
	OL7	12.53	0.59	1.15	0.15
	OL8	104.09	7.70	6.56	0.68
Saprolitic ores	OS1	1.31	0.09	0.39	0.02
	OS2	2.46	0.18	0.72	0.08
	OS3	1.27	0.15	0.44	0.13
Sediments	Se1	1.57	0.03	20.89	5.50
	Se2	10.06	1.60	0.62	0.17
	Se3	2.37	1.84	1.49	0.71

*Limit of detection (LoD) Cr = 0.1 mg kg^{-1}

Table 3 Major and trace cations and anions, alkalinity and dissolved organic carbon (DOC) in dissolved fraction of water samples. Suspended particulate matter (SPM) and carbon (C) content in filters. Conductivity, temperature and pH values at time of sampling.

Element		Stream2	Pond1	Pond2	Pond3	Mining area Piezo 1 (before mine)	Piezo 2 (after mine)	Piezo 3 (before smelter)	Piezo 4 (after smelter)	Pristine area Stream1
Major elements (mg L^{-1})	K	0.05	0.13	0.32	0.29	0.22	0.16	2.80	1.06	0.02
	Mg	7.99	6.69	13.13	7.25	23.90	20.05	17.21	1.31	11.81
	Ca	0.87	1.28	5.06	1.13	0.67	1.79	31.70	3.36	2.54
	Na	0.25	0.32	0.17	0.43	0.22	0.19	10.11	3.78	0.55
Trace elements (µg L^{-1})	Fe	1.09	4.91	3.68	2.16	1.69	0.36	2.20	1.25	242
	Mn	6.17	1.43	<LoD	0.81	0.84	0.09	1.20	79	86
	Al	0.73	0.32	1.42	1.31	7.49	4.37	1.31	0.90	<LoD
	Cr	13	757	58	89	2.39	0.21	1.09	0.16	0.09
	Ni	76	14.21	9.52	7.48	12	0.91	1.96	11.07	37
	Sr	1.91	1.36	2.85	1.26	1.29	2.51	94	8.13	5.23
	Zn	1.60	18	3.87	19	18	0.93	10.57	56	2.78
Anions (µg L^{-1})	F^-	< LoD	32	61	n.d.	99	60	254	53	< LoD
	Cl^-	330	436	1604	n.d.	447	393	820	2990	359
	NO_3^-	726	3352	353	n.d.	5042	24	419	4007	260
	SO_4^{2-}	97	1884	1385	n.d.	729	2441	2986	168	55
$\delta^{53}Cr$ (‰)		2.10	2.62	3.66	n.d.	n.d.	n.d.	2.18	2.19	2.60
DOC (mg L^{-1})		1.66	2.03	2.31	5.48	3.74	4.65	2.94	2.28	1.78
Alkalinity (mg L^{-1})		29	15	37	15	50	54	79	11	29.77
SPM (mg L^{-1})		3	166	316	176	5	8	8	18	1.08
Particulate Organic Carbon (wt %)		1.6	1.18	0.64	1.13	5.86	5.01	6.51	9.63	3.65
Temperature (°C)		23.3	22.2	26.5	26.1	27.8	25.8	25.3	27.2	24.4
Conductivity (µS cm^{-1})		60	58	105.6	62.6	166.7	155	292	48.3	96.2
pH		7.5	7.5	8.3	7.8	7.4	9.2	6.6	5.7	7.4

* Limit of detection (LoD) F^- = 20 µg L^{-1}; NO_3^- = 20 µg L^{-1}

n.d.= not determined